

BULK GROWTH AND CHARACTERIZATION OF CADMIUM ZINC  
TELLURIDE CRYSTALS FOR MERCURY CADMIUM TELLURIDE  
INFRARED DETECTOR APPLICATIONS

A THESIS SUBMITTED TO  
THE GRADUATE SCHOOL OF NATURAL AND APPLIED SCIENCES  
OF  
MIDDLE EAST TECHNICAL UNIVERSITY

BY

HASAN YASİN ERGUNT

IN PARTIAL FULFILLMENT OF THE REQUIREMENTS  
FOR  
THE DEGREE OF MASTER OF SCIENCE  
IN  
MICRO AND NANOTECHNOLOGY

SEPTEMBER 2012

Approval of the Thesis:

**BULK GROWTH AND CHARACTERIZATION OF CADMIUM ZINC  
TELLURIDE CRYSTALS FOR MERCURY CADMIUM TELLURIDE  
INFRARED DETECTOR APPLICATIONS**

Submitted by **HASAN YASİN ERGUNT** in partial fulfillment of the requirements  
for the degree of **Master of Science in Micro and Nanotechnology Department,**  
**Middle East Technical University** by,

Prof. Dr. Canan Özgen  
Dean, Graduate School of **Natural and Applied Sciences**

\_\_\_\_\_

Prof. Dr. Mürvet Volkan  
Head of Department, **Micro and Nanotechnology**

\_\_\_\_\_

Prof. Dr. Raşit Turan  
Supervisor, **Physics Dept., METU**

\_\_\_\_\_

Prof. Dr. Cengiz Beşikci  
Co-Supervisor, **Electrical and Electronics Eng. Dept., METU**

\_\_\_\_\_

**Examining Committee Members:**

Prof. Dr. Mehmet Parlak  
Physics Dept., METU

\_\_\_\_\_

Prof. Dr. Raşit Turan  
Physics Dept., METU

\_\_\_\_\_

Prof. Dr. Cengiz Beşikci  
Electrical and Electronics Eng. Dept., METU

\_\_\_\_\_

Assist. Prof. Dr. Yunus Eren Kalay  
Metallurgical and Materials Eng. Dept., METU

\_\_\_\_\_

Dr. Süleyman Umut Eker  
Electrical and Electronics Eng., PhD., ASELSAN, Inc.

\_\_\_\_\_

**Date: 13.09.2012**

**I hereby declare that all information in this document has been obtained and presented in accordance with academic rules and ethical conduct. I also declare that, as required by these rules and conduct, I have fully cited and referenced all material and results that are not original to this work.**

Name, Last name : Hasan Yasin Ergunt

Signature :

# ABSTRACT

## BULK GROWTH AND CHARACTERIZATION OF CADMIUM ZINC TELLURIDE CRYSTALS FOR MERCURY CADMIUM TELLURIDE INFRARED DETECTOR APPLICATIONS

Ergunt, Hasan Yasin

M. Sc., Micro and Nanotechnology Department

Supervisor : Prof. Dr. Raşit Turan

Co-Supervisor : Prof. Dr. Cengiz Beşikci

September 2012, 86 pages

HgCdTe (MCT) infrared (IR) photodetectors have been used for various military and civilian applications including thermal imaging, medical imaging, and astronomy. These detectors are commonly fabricated on MCT layers grown on a foreign substrate epitaxially using delicate growth techniques such as Molecular Beam Epitaxy (MBE). The crystal quality of epitaxial layers grown on a substrate critically depends on the quality of the substrate. One of the stringent requirements in choosing the substrate material is the lattice match between grown layer and the underlying substrate. With perfectly matching lattice structure, CdZnTe has been the major substrate material for the MCT growth. The production of defect free single crystal CdZnTe bulk crystal has then attracted great attention among the research and industrial community of MCT based photodetectors.

This thesis focuses on the growth and characterization of  $Cd_{1-x}Zn_xTe$  crystals with the main objective of obtaining high-quality, CZT bulk crystal with large crystal sizes. To be compatible with the subsequent MCT growth, we aimed to obtain  $Cd_{0.96}Zn_{0.04}Te$  crystals with (211) crystal surface orientation. CdZnTe bulk crystal

growths were performed in three-zone vertical Bridgman furnace by a high temperature melt process called “Modified Bridgman Technique”.

Difficulties in both growth and characterization are presented and discussed in this report. Characterization of the grown CdZnTe crystal was performed to determine the crystallographic orientation, crystal quality, Zn distribution, IR transmission, resistivity, polarity, etch pit density, and surface properties. For this purpose, electron microscopy with analytical diagnostic tools like EDS and EBSD, XRD, optical transmission spectroscopy, and electrical measurement systems have been employed.

We demonstrated the successful growth of single crystal CZT crystals using our simple Bridgman furnace. Physical properties of the grown crystal were very promising and encouraging for future applications. Crystal pieces having sizes larger than  $5 \times 5 \text{ mm}^2$  with uniform Zn distribution and (211) surface orientation were obtained. IR transmission of nearly 60% which is as good as that of the commercial substrates was achieved. The electrical resistivity was much better (higher) than generally accepted values. However, the XRD results indicated the presence of defects and/or micro grains in the bulk crystal. These structures seemed to have prevented obtaining good FWHM values, which are the measure of crystal quality, in the XRD analysis.

**Keywords:** CdZnTe, bulk growth, Bridgman technique, HgCdTe, substrate

# ÖZ

## CIVA KADMIYUM TELLÜR KIZILÖTESİ DEDEKTÖR UYGULAMALARI İÇİN KADMIYUM ÇİNKO TELLÜR KRİSTALLERİNİN HACİMSEL BÜYÜTÜLMESİ VE KARAKTERİZASYONU

Ergunt, Hasan Yasin

Yüksek Lisans, Mikro ve Nanoteknoloji EABD  
Tez Yöneticisi : Prof. Dr. Raşit Turan  
Ortak Tez Yöneticisi : Prof. Dr. Cengiz Beşikci

Eylül 2012, 86 sayfa

HgCdTe (MCT) kızılötesi fotodedektörler termal görüntüleme, medikal görüntüleme ve astronomi gibi askeri ve sivil uygulamalarda kullanılır. Bu dedektörler moleküler ışın epitaksisi (MBE) gibi gelişmiş büyütme teknikleri kullanılarak alttaş üzerine epitaksiyel olarak büyütülmüş MCT katmanlarıyla üretilir. Alttaş üzerine büyütülen epi-katmanların kristal kalitesi alttaşın kalitesine bağlıdır. Alttaş malzemesini belirlemek için en önemli gerekliliklerden biri de epi-katman ile alttaş arasındaki örgü uyumudur. CdZnTe örgü uyumuyla MCT epi-katmanları için temel bir alttaş malzemesi olmuştur. MCT tabanlı kızılötesi fotodedektör teknolojisini geliştiren araştırma grupları için yüksek kalitede CdZnTe külçe elde edilmesi bir hayli önem kazanmıştır.

Bu tez çalışması, yüksek kalitede  $Cd_{1-x}Zn_xTe$  kristallerinin üretim ve karakterizasyon çalışmaları üzerine yoğunlaşmıştır. MCT epi-katman büyütülmesi ile uygun olacak şekilde (211) kristal yönelimine sahip  $Cd_{0.96}Zn_{0.04}Te$  alttaşlarının üretilmesi hedeflenmiştir. CdZnTe hacimsel büyütme için üç sıcaklık bölmeli dikey Bridgman fırınında “değiştirilmiş Bridgman tekniği” kullanılarak gerçekleştirilmiştir.

Üretim ve karakterizasyon işlemleri sırasında karşılaşılan zorluklar gösterilmiştir. Elde edilen CdZnTe kristalleri, kristal yönelimi, kristal kalitesi, Zn dağılımı, kızılötesi geçirgenliği, özdirenç, kristal polaritesi, defekt yoğunluğu ve yüzey özelliklerini belirlemek için karakterize edilmiştir. Bu amaçla EDS ve EBSD gibi elektron mikroskobu analizleri, XRD ölçümleri, optik spektroskopi ölçümleri ve elektriksel ölçümler gerçekleştirilmiştir.

Bridgman fırınında gerçekleştirilen başarılı CdZnTe büyütme gösterilmiştir. Geliştirilen CdZnTe kristallerinin özellikleri gelecekteki CZT çalışmaları için umut verici olmuştur. Yürütülen çalışmalar sonucunda 5 x 5 mm<sup>2</sup>'den daha büyük boyutlarda, homojen Zn dağılımına ve (211) kristal yönelimine sahip CZT kristalleri elde edilmiştir. Ticari alttaşlar ile benzer şekilde %60'a yakın bir kızılötesi geçirgenlik değerine ulaşılmıştır. Özdirenç değeri 10<sup>7</sup> Ωcm olarak ölçülmüştür. Ancak XRD ölçümü sonuçlarına göre defektlerin ve subgrainlerin olduğu gözlenmiştir. XRD analizlerinde bu yapıların CZT kristal kalitesini etkilediği ve yüksek FWHM değerlerinin elde edilmesine neden olduğu görülmüştür.

**Anahtar kelimeler:** CdZnTe, hacimsel büyütme, Bridgman tekniği, HgCdTe, alttaş.

*To my lovely family,  
and two little friends; Mirni and Pamuk*

## ACKNOWLEDGEMENTS

I would like to thank my thesis advisor Prof. Dr. Raşit Turan for his endless support and providing me a key role throughout this study. I am very grateful to him for his enlightened guidance as well as provided experience in many sophisticated laboratories. I really appreciate him for giving me chance to meet valuable science people, and to operate valuable analysis instruments. He always trusted me and resolved any problem that I have encountered in both daily and academic life.

I would like to thank Prof. Dr. Cengiz Beşikci for his supportive attitude and patience during the CZT studies. I am very grateful to him for his hospitality in Quantum Devices and Nanophotonics Research Laboratory and providing me to operate high resolution XRD instrument throughout my study.

I gratefully thank Prof. Dr. Mehmet Parlak for his guidance and collaboration. I really appreciate his support, helpful discussions and kindness. I am also grateful to him for sharing his deep experience in semiconductor area. Without his guidance and knowledge, I could never progress in crystal growth.

Special thanks go to Dr. Süleyman Umut Eker for his guidance and sharing deep knowledge in HgCdTe growth technology. I am also delightful for his valuable suggestions about characterization techniques and his encouraging comments throughout my study. I also thank him for his patience during the one-day lasting XRD analyses.

I would like to thank Assistant Prof. Dr. Yunus Eren Kalay for sharing his deep experience in EBSD studies. He was always supportive during the single crystal analyses. Without his promising EBSD trials, I could never checked the single crystallinity of CZT slices.

I would like to thank Alp Tolungüç for his valuable comments about almost all the steps throughout the study. Especially, with his help, I learnt the basics of professional academic study and recent technology device applications. I thank him for his careful work in dicing our slices and I really appreciate his great friendship.

I would like to thank Ayşe Şan for her priceless work in chemical etching processes and her great friendship. Her valuable contribution to the etching procedures was really helpful for our defect studies.

I really appreciate Burak Aşıcı for his deep knowledge in both HgCdTe and CdZnTe growth technologies. His crucial comments and suggestions helped us to progress in material growth and characterization.

I gratefully thank Ümid Tümkaya for his guidance and support throughout this research study. Specifically, his suggestions about proper documentation were really helpful during the preparation of this thesis.

I would like to thank ASELSAN Inc. for their support and funding in this study. My sincere thanks are to Electronics Design Manager Mrs. Hacer Selamoğlu for her encouraging support and deep interest in this research study.

I really appreciate Seçkin Öztürk for his great work in SEM imaging and ingot slicing. I am very delightful for his SEM training sessions and his excellent friendship. His valuable help has improved the prominent part of my thesis study.

I would like to thank also Sedat Canlı for his contributions to the EBSD studies. He was always supportive and shared my motivation and excitement throughout the study. I appreciate his friendship and his funny jokes.

My sincere thanks are to Kutlu Kutluer for his great friendship and support. I also thank Dr. Tunay Tansel for his kindness and his supportive behavior. I also thank both for excellent lunch times.

I also thank Dr. Mustafa Kulakçı for his deep knowledge in semiconductor technology. He is always supportive and it is an honour to have his friendship.

My special thanks go to Olgu Demirciođlu, Mehmet Karaman, Fırat Es, İrem Tanyeli, Erdem Katı, Ayşe Banu Kosif, Urcan Güler, Döndü Şahin, Selçuk Yerci, Burcu Altuntaş, Serim İlday, Emine Hande Çiftpınar, Yücel Eke and all Semiconductor Materials and Devices Group for their support and friendship.

I gratefully thank Adem Yenisoy, Yaman Çankaya, Yağız Çankaya, Bilginur Maraş, Nuri Özer, and Mehmet Karayel for their excellent friendship and endless support throughout my study.

Finally, I would like to thank to my all family for their support and encouragement throughout my life.

# TABLE OF CONTENTS

ABSTRACT .....	iv
ÖZ .....	vi
ACKNOWLEDGEMENTS .....	ix
TABLE OF CONTENTS .....	xii
LIST OF TABLES .....	xv
LIST OF FIGURES .....	xvi
CHAPTERS	
1. INTRODUCTION .....	1
1.1 Scope .....	1
1.2 IR Radiation .....	3
1.3 Detecting IR Light.....	3
1.4 Development of HgCdTe Detector Technology and Material Properties of HgCdTe .....	4
1.4.1 Development of HgCdTe Detector Technology .....	4
1.4.2 Material Properties of HgCdTe.....	5
1.5 Substrates for HgCdTe Epitaxial Growth .....	6
2. BULK GROWTH OF CADMIUM ZINC TELLURIDE .....	8
2.1 Introduction .....	8
2.2 Material Properties of CdZnTe.....	8
2.2.1 Structural Properties .....	9
2.2.2 Thermal Properties.....	10

2.3 CdZnTe Growth Techniques .....	11
2.3.1 Bridgman Technique.....	12
2.3.2 Traveling Heater Method (THM) .....	14
2.3.3 Vertical Gradient Freeze (VGF) .....	15
2.4 Experimental Details – Bulk Growth of CdZnTe in Three-Zone Vertical Bridgman Furnace .....	15
2.4.1 Selection of Crucible Material .....	16
2.4.2 Designs of Silica Growth Ampoule and pBN Crucible.....	17
2.4.3 Preparation and Homogenization of Starting Charge .....	19
2.4.4 Bridgman Session of CdZnTe Crystal Growth.....	23
2.5 Conclusions .....	24
3. CADMIUM ZINC TELLURIDE WAFER PROCESSING .....	26
3.1 Introduction .....	26
3.2 Ingot Slicing .....	27
3.3 Lapping.....	29
3.4 Grain Revealing and Dicing .....	31
3.5 Lapping and Mechanical Polishing .....	32
3.6 Chemical Etching .....	33
3.7 Inspection .....	34
4. CADMIUM ZINC TELLURIDE CHARACTERISTICS AS SUBSTRATES FOR THE EPITAXIAL GROWTH OF MERCURY CADMIUM TELLURIDE.....	35
4.1 Introduction .....	35
4.2 Purity, Inclusions, and Precipitates in CdZnTe .....	35
4.3 Zn Distribution in CdZnTe Wafers .....	37
4.4 Infrared Transmission.....	38
4.5 Crystallographic Surface Orientation .....	40
4.6 X-ray FWHM and Crystallographic Misorientation .....	41

4.6.1 X-ray FWHM.....	41
4.6.2 Crystallographic Misorientation .....	43
4.7 Polarity Determination of CZT Wafers .....	43
4.8 Etch-Pit Density (EPD) Measurements of CdZnTe Substrates.....	45
4.9 Resistivity of CdZnTe Substrates.....	46
4.10 Surface Roughness and Surface Oxidation of CdZnTe Wafers .....	46
4.10.1 Surface Roughness.....	46
4.10.2 Surface Oxidation .....	47
4.11 Total Thickness Variation .....	47
4.12 Conclusions .....	47
5. CHARACTERIZATION OF GROWN CADMIUM ZINC TELLURIDE CRYSTALS .....	49
5.1 Introduction .....	49
5.2 Zinc Distribution Mapping of CdZnTe Wafers.....	50
5.3 Infrared Transmission.....	57
5.4 Polarity Determination of Grown CdZnTe Wafers .....	62
5.5 Etch-Pit Density Measurements of CdZnTe Wafers .....	62
5.6 Resistivity Measurements of Grown CdZnTe Wafers .....	68
5.7 Crystallographic Surface Orientation Measurements.....	69
5.7.1 Surface Orientation Measurements by XRD .....	69
5.7.2 Surface Orientation Measurements by EBSD .....	72
5.8 X-ray Rocking Curve Measurement.....	74
5.9 Crystallographic Misorientation Analysis .....	75
5.10 Conclusions .....	78
6. CONCLUSION AND FUTURE STUDIES .....	79
REFERENCES.....	82

## LIST OF TABLES

### TABLES

Table 2.1. Temperatures and times followed during the homogenization process ....	22
Table 3.1 Size of diamond particles in lapping films used and .....	31
Table 5.1 Zn distribution of the commercial CdZnTe substrate of Chinese origin ...	51
Table 5.2 Zn distribution of CZT-4_1 slice grown at METU .....	53
Table 5.3 Zn distribution of CZT-5_1 sample grown at METU .....	55
Table 5.4 Zn distribution of CZT-7_1 sample grown at METU .....	55

# LIST OF FIGURES

## FIGURES

Figure 1. 1 Bandgap and lattice const. variation of various semicond. compounds ....	7
Figure 2.1 Lattice const. (a) versus x and y diagram in CZT and MCT, at 300 K ....	10
Figure 2.2 (a) Cd-Te bin phase diag. (b) Sol-liq. interf. of Cd-Zn-Te tern system....	11
Figure 2.3 Basic temperature fashion followed in Bridgman systems.....	13
Figure 2.4 Schematic of THM method growth system .....	14
Figure 2.5 Technical drawings of pBN crucibles designed at METU .....	17
Figure 2.6 Technical drawings of pBN crucibles designed at METU .....	18
Figure 2.7 Designed silica growth ampoules used for sealing prior to growth.....	19
Figure 2.8 Vertical homogenization furnace with rocking apparatus .....	20
Figure 2.9 Three-zone vertical Bridgman furnace .....	23
Figure 3.1 Schematic flow of CdZnTe wafer processing .....	27
Figure 3.2 Diamond lapping films and microscope image of diamond particles .....	32
Figure 4. 1 Carrier concent. dependence on IRT of (a) CZT crystals, (b) p-type, and n-type ingots .....	39
Figure 4. 2 Schematic of a general FWHM concept.....	42

Figure 4. 3 Cd-terminated and Te-terminated surfaces.....	44
Figure 5.1 Commercial CZT substrate with Chinese origin (20 x20 mm <sup>2</sup> ).....	51
Figure 5.2 Obtained slice (named CZT-4_1) from the ingot CZT-4 .....	52
Figure 5.3 (a) CZT-5_1 slice, (b) CZT-7_1 slice.....	54
Figure 5.4 Zn distribution tendency of samples CZT-5_1 and CZT-7_1 .....	56
Figure 5.5 IR transmission of 850μm-thick CZT-4_1 slice.....	57
Figure 5.6 IR transmission of 850μm-thick CZT-5_2 sample.....	58
Figure 5.7 IR transmission of 830μm-thick CZT-7_1 sample.....	60
Figure 5.8 IRT of 820μm-thick commercial CZT wafer with Chinese origin.....	61
Figure 5.9 IR transmission of 820μm-thick CZT-5_1 sample.....	61
Figure 5.10 Etch-pit formation on CZT-6_1 slice .....	63
Figure 5.11 Hexagonal or round-like pits formed on CZT-6_1 slice .....	64
Figure 5.12 Etch pattern formed on CZT-5_3 after Everson etching .....	65
Figure 5.13 Etch pattern formed on CZT-5_4 after Everson etching + Br <sub>2</sub> -MeOH ..	66
Figure 5.14 Etch pattern formed on CZT-5_5 after E-reagent exposure .....	67
Figure 5.15 Current-Voltage characteristics of CZT-5_6 at 77K .....	68
Figure 5.16 X-ray diffraction spectrum of CZT-7_2 slice.....	70

Figure 5.17 X-ray diffraction spectrum of CZT-7_1 prototype.....	71
Figure 5.18 EBSD map of CZT-7_1 slice shown in the SEM picture. ....	72
Figure 5.19 SEM image of CZT-7_1 prototype.....	73
Figure 5.20 Inverse pole figure (IPF) map of CZT-7_1.....	74
Figure 5.21 Misorientation angle distribution of CZT-7_1 prototype .....	76
Figure 5.22 100 $\mu$ m-scaled noise free and single crystalline selected area.....	76
Figure 5.23 Misorientation angle distribution of CZT-7_1 prototype .....	77
Figure 5.24 40 $\mu$ m-scaled area and misorientation angle distribution of CZT-7_1 sample in reference to (211) crystal orientation .....	78

# CHAPTER I

## INTRODUCTION

### 1.1 Scope

HgCdTe (MCT) IR photodetectors have been intensively used in various applications since the first synthesis of HgCdTe material in 1958 [1]. Today, with the excellence in performance in the mid and long wavelength infrared region, it has reached an unbeatable position for these applications. However, difficulties arising from the growth of defect-free MCT layers with desired chemical composition needed to be overcome to implement this technology to real applications. Many research groups at universities and companies have been struggling with the problems related to epitaxial growth, detector fabrication, focal plane array (FPA) production, and read out circuitry (ROIC) needed to fabricate end products [2]. One of the issues in growing high quality MCT crystal is the lack of an appropriate substrate lattice-matched with the MCT epilayer. Having almost the same lattice constant with that of MCT,  $\text{Cd}_{0.96}\text{Zn}_{0.04}\text{Te}$  offers an excellent platform to grow layers upon it [3]. The first synthesis of CdZnTe material was performed in mid-1980s following the first synthesis of CdTe in mid 1970s [2]. Later, CZT material became highly critical for the epitaxial growth of MCT due to perfect lattice-match. For high quality CZT substrates, state-of-the-art techniques for bulk growth of CdZnTe were developed. However, limits on the maximum wafer size, high production cost, and inhomogeneity of the lattice constant (i.e. varying composition throughout the CZT

wafer surface) [3] are still serious problems that should be addressed and solved with new research studies.

Throughout this study, material development of CdZnTe and characterization of the grown CdZnTe material were intensively investigated. The overview of this thesis work can be summarized with the main objectives as follows:

- The first part of this study, Chapter 1, introduces the main concepts and basics of IR radiation and detection. In order to emphasize the importance of CdZnTe substrates, HgCdTe IR detector technology is presented in brief.
- The second part of the work, Chapter 2, is dedicated to the bulk growth of CdZnTe. Mainly, bulk growth techniques are summarized. As an experimental part, growth technique used in this study, and specified growth parameters are explained in detail.
- The third part of the thesis, Chapter 3, is composed of wafer processing steps. These steps including slicing and polishing are provided subsequently in each section. Wafer processing steps followed in this study are also explained in each wafer processing step as an experimental detail.
- In Chapter 4, characteristics of high quality, commercial CdZnTe substrates are handled in detail. Discussion on purity, compositional analysis, infrared transmission, crystal orientation, crystal quality, and electrical resistivity are presented. Most of characterization techniques present in literature are also explained in Chapter 4.
- Chapter 5 focuses on the discussion of the results we obtained from CZT crystals grown in this study. We present structural, chemical, electrical, and optical properties of samples produced.
- In Chapter 6, a general conclusion to the whole thesis work is provided. Significant parts of the study and outcomes of the experiments are highlighted. Finally, recommendations for future work are outlined.

## 1.2 IR Radiation

Any object radiates above 0 K, and radiation is emitted and absorbed by objects. This is because the molecular excitation increases even if the temperature increases slightly. This molecular excitation causes electrical charge carriers to accelerate, which results in generation of radiation [4]. This radiation energy is related to the wavelength, Planck's constant and the speed of light, and given by the known equation  $W=hc/\lambda$ . The radiation emitted by a blackbody is determined by Planck's Law.

$$M_e = \frac{2 \cdot \pi \cdot h \cdot c^2}{\lambda^5 \cdot \left\{ \exp\left(\frac{h \cdot c}{\lambda \cdot k \cdot T}\right) - 1 \right\}} \left[ \frac{W}{\mu m \cdot m^2} \right] \quad (1.1)$$

In the electromagnetic spectrum, 0.7 $\mu$ m - 1000 $\mu$ m region belongs to IR radiation. In the case of HgCdTe-based IR photodetectors requiring high quality CdZnTe substrates, specific wavelength intervals for which the atmosphere is almost transparent are considered. The term "atmospheric window" is widely used for these wavelength intervals. The thermal imaging in the field can only be performed in these windows. There are two major atmospheric windows called mid wave infrared (MWIR) band with the wavelength range of 3-5  $\mu$ m, and long wave infrared (LWIR) band with the wavelength range of 8-12  $\mu$ m. The optical response of the photodetectors should conform to these optical wavelength intervals [5].

## 1.3 Detecting IR Light

In a broad sense, infrared light detection is achieved by two types of detectors: photon detectors and thermal detectors. Apparently, these detectors are classified in terms of transduction mechanisms. In the photon detectors case, direct interaction of the optical radiation with the atomic lattice of material takes place; whereas, the

thermal detectors are based on the response to the heat generated by the absorbed energy of the optical radiation [6]. Since our primary interest is MCT-based IR photodetector, thermal detectors are not to be discussed.

Photon detectors are classified into two types as photoconductors and photodiodes. Basically, in both photoconductors and photodiodes, conventional detection mechanism is based on the excitation from valence band to conduction band in a semiconductor material. Here, the excitation is achieved by photons.

## **1.4 Development of HgCdTe Detector Technology and Material Properties of HgCdTe**

### **1.4.1 Development of HgCdTe Detector Technology**

Development of HgCdTe detector technology is of higher priority for thermal imaging. Due to the critical importance in the military applications, defense industry has provided significant support to the growth of MCT technology through the years, and the prominent scientific knowledge and the technological experience have been achieved by this support. On the other hand, the literature on MCT technology has always been under the pressure of confidentiality. This has created restrictions preventing the international collaboration among research groups [2].

IR imaging is widely used in many areas such as, night vision, search and rescue, isolation of buildings against heat losses, medical imaging, and astronomy. In 1958, HgCdTe was first synthesized by Lawson's research group in Royal Radar Establishment, England. This first synthesized HgCdTe was intended to be used for detection of radiation in LWIR band [2].

Next, advanced applications in crystal growth and epitaxial growth technologies led to high quality detector material and advanced characterization techniques [7].

MCT detector technology can be classified as three generations:

- First generation MCT photodetectors, photoconductive linear arrays
- Second generation MCT photodetectors, 2-dimensional photovoltaic devices
- Third generation MCT photodetectors, second generation detectors having increased performance in detectivity and very large format size. Dual-band or multi-spectral photodetectors, and hyperspectral arrays [2, 3].

Following the development of second generation MCT photodetectors, MCT-based IR detector technology has shown a crucial development with the production of large detector arrays (>128x128) [2].

Surface passivation which was a serious problem for second generation MCT photodetectors until 1987. In 1987, this problem was solved by using CdTe passivation, which led to the production of larger-scale productions [2].

Finally, the third generation MCT photodetectors are of state-of-the-art technology today. Currently, the largest IR FPA is of 2048 x 2048 pixels [3] and even multi-color systems are readily available in the commercial market [8].

#### **1.4.2 Material Properties of HgCdTe**

Superior material properties such as high absorption coefficient, direct bandgap, moderate thermal expansion coefficient and dielectric constant, longer lifetime of free carriers make HgCdTe ternary compound an ideal IR material [9]. Moreover, MCT-based photodetectors can be operated at relatively higher temperatures when compared to other IR detector systems such as QWIPs. Depending on the x value (i.e. Cd mole fraction) in the  $\text{Hg}_{1-x}\text{Cd}_x\text{Te}$  structure, bandgap of HgCdTe can be modulated to operate within 1-30  $\mu\text{m}$  wavelength interval. As in the case of other IR detector systems, HgCdTe has its own advantages and disadvantages. For instance, it

is reported that while HgCdTe focal plane arrays are of higher quantum efficiency, higher operating temperature, and higher performance than the QWIPs have, QWIPs offer high yield fabrication, higher operability, better uniformity, and lower cost. In addition, in MCT case, for LWIR band applications, the production yield of MCT epilayers is known to be low; and therefore, the production cost is dramatically higher in this case [3, 10]. Current HgCdTe detector technology aims to obtain larger FPA production, increase the reliability, reproducibility and reduce the cost [9]. This is possible by improving the material properties of the substrates. One of the major issues is finding the most appropriate substrate for the MCT crystal growth. In the following section, we summarize the studies on the substrates for the MCT growth.

## **1.5 Substrates for HgCdTe Epitaxial Growth**

MCT layers are commonly produced by an epitaxial growth process in Molecular Beam Epitaxy (MBE) reactors. It is well known that the lattice constant of the epilayers should match the lattice constant of the substrate for the production of high quality epilayer. Otherwise, the defects formed at the interface due to the lattice mismatch are transferred into the grown layer, which degrades the performance of the device made on it. Lattice constant of HgCdTe depends on the x value in  $\text{Hg}_{1-x}\text{Cd}_x\text{Te}$  [9]. This dependence and the candidate materials as substrate are shown in figure 1.1.

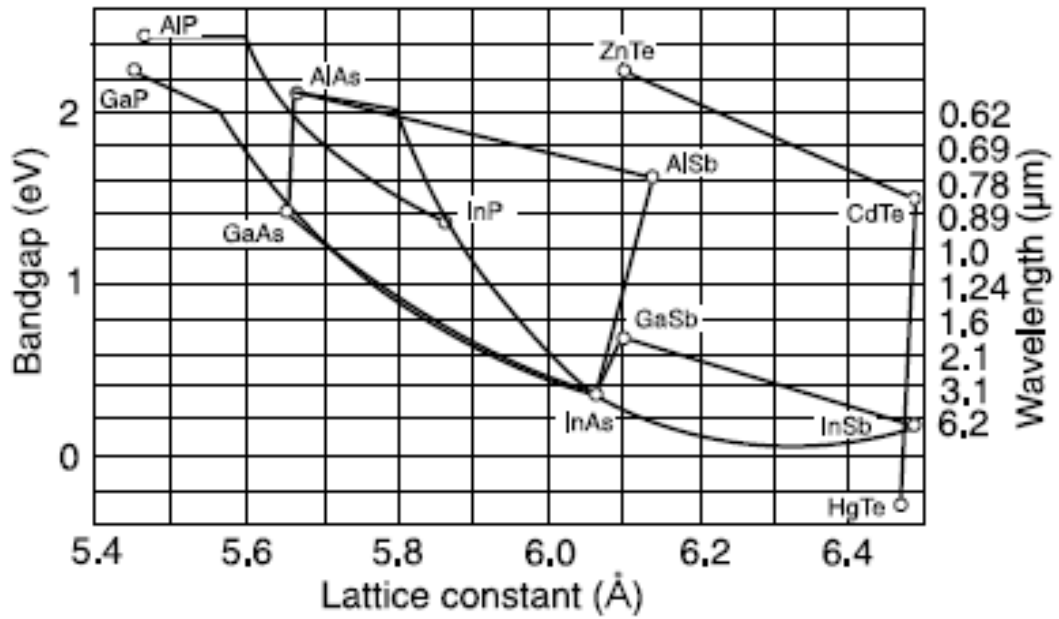


**Figure 1.1** Bandgap and lattice constant variation of various semiconductor compounds [2]

We see that the lattice constant of  $\text{Cd}_{0.96}\text{Zn}_{0.04}\text{Te}$  matches with the lattice constant of MCT very well. For this reason,  $\text{CdZnTe}$  has been the most successful substrate for the epitaxial growth of MCT layers. However, recent studies have shown that alternative substrates such as Si offers significant cost advantage [9]. In this case, the problems originating from defects formed due to the lattice mismatch should be solved or at least minimized for certain applications.

## **CHAPTER II**

### **BULK GROWTH OF CADMIUM ZINC TELLURIDE**

#### **2.1 Introduction**

An iconic example of II-VI compound system, CdZnTe, is still primary choice as the substrate material for the epitaxial growth of IR material, HgCdTe; although serious difficulties encountered during the bulk growth process of CZT. However, these difficulties or problems are minimized and even overcome with the advance in materials science as Dr. Sekimoto, prominent scientist and entrepreneur says “Who dominates materials, dominates technology.” In order to study and understand a material from II-VI family, one requires to have knowledge of related material properties in detail [11]. This chapter deals with CdZnTe properties, growth techniques of CdZnTe, and bulk growth of CdZnTe as experimental details of the part of the work.

#### **2.2 Material Properties of CdZnTe**

Before starting to discuss the bulk growth of CdZnTe material, it is required to define some of the crystal and thermal properties commonly used in bulk-growth. Here, as a structural property, (211) crystal orientation is to be emphasized due to its prominence in epitaxial growth of HgCdTe in MBE, and related thermal properties

are also to be presented. Since the  $\text{Cd}_{1-x}\text{Zn}_x\text{Te}$  semiconductor alloy is composed of proper ratios of CdTe and ZnTe, which are indeed  $(\text{CdTe})_{1-x}$  and  $(\text{ZnTe})_x$ , structural and thermal properties of CdTe, ZnTe, and CdZnTe will be presented.

### 2.2.1 Structural Properties

Since the lattice-matching of CZT substrates is the primary requirement of successful epitaxial growth of MCT, lattice constant ( $a$ ) values of CdTe and ZnTe are specified as 6.481 Å and 6.1037 Å, respectively [7]. The ‘x’ value in  $\text{Cd}_{1-x}\text{Zn}_x\text{Te}$  alloy determines the lattice constant and it is specified as:

$$a (\text{Å}) = 6.4810 - 0.3773x \quad (2.1)$$

CdZnTe is formed by the zincblende arrangement of CdTe and ZnTe. The zincblende structure is based on the cubic space group  $F43m$ . According to the relation 2.1, the lattice constant ( $a$ ) is x-dependent for  $\text{Cd}_{1-x}\text{Zn}_x\text{Te}$ . Very similar case is also valid for  $\text{Hg}_{1-x}\text{Cd}_x\text{Te}$ . CdTe is still not the first choice as an epitaxial substrate material due to its large lattice-mismatch with  $\text{Hg}_{1-x}\text{Cd}_x\text{Te}$ , although it is much lower when compared to Si and GaAs [9]. This lattice-mismatch problem was overcome by the addition of Zn in proper mole fraction (i.e.  $x=0.04$ ) into CdTe. MCT epilayers are almost perfectly lattice matched with  $\text{Cd}_{0.96}\text{Zn}_{0.04}\text{Te}$  substrates [2]. The x value, the Zn composition in CZT, is highly vital in MCT Epitaxy (Figure 2.1). Besides, it is not the sole requirement for the epitaxial growth of MCT epilayers.

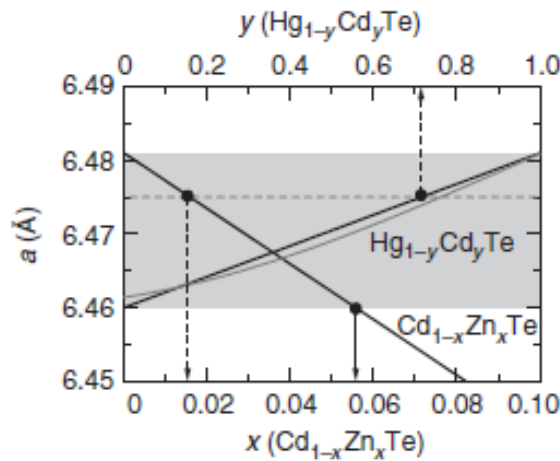


**Figure 2.1** Lattice constant (a) versus x and y diagram in CZT and MCT, respectively, at 300 K [9].

Figure 2.1 shows the lattice-match conditions between MCT and CZT corresponding to the x and y values. In general,  $y = Ax$  (where A is a constant) can be obtained from the diagram. It should be also noticed that the growth temperatures vary depending on the growth method to conform the critical lattice-matching conditions. The growth temperatures for different methods are 450-500 °C for LPE, 350 °C for MOVPE, and 190-200 °C for MBE [9].

### 2.2.2 Thermal Properties

As a thermal property, phase diagram is to be handled due to its importance in bulk-growth. Literally, phase diagram is somewhat a guide for crystal growth of a specific material. For CdZnTe or mainly for CdTe, phase diagram shows the curves of solid-liquid interface (Figure 2.2).

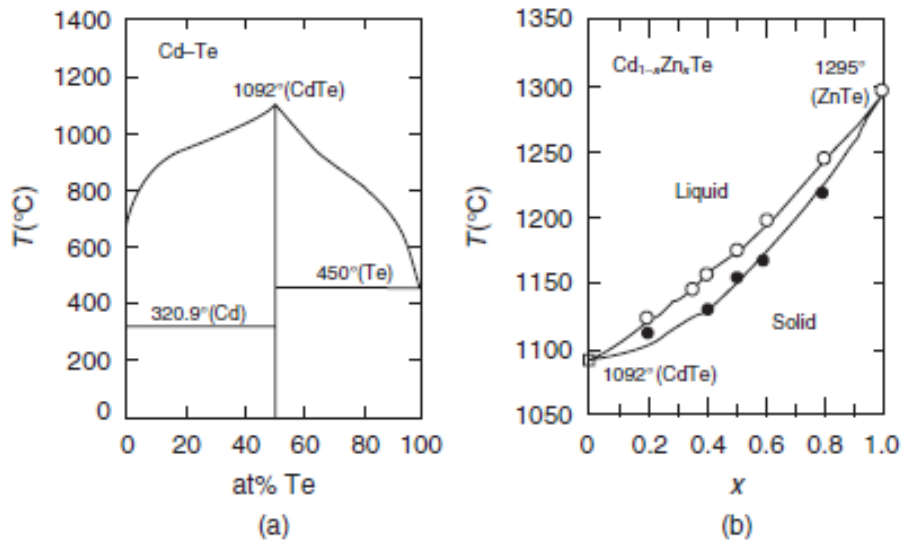


**Figure 2.2** (a) Cd-Te binary phase diagram. (b) Solid-liquid interface curves of Cd-Zn-Te ternary system [9]

There exist other thermal properties such as specific heat, Debye temperature, thermal expansion coefficient, thermal conductivity, and thermal diffusivity other than phase diagram [7, 9]. However, these thermal properties are not to be considered here in detail since these are beyond our scope.

### 2.3 CdZnTe Growth Techniques

Various growth techniques have been developed following the first synthesis of CdZnTe material. Since then, many research groups and institutions have conducted crucial growth studies and mature growth techniques have been revealed. In the last decade, prominent improvements in CZT growth have been achieved in terms of reduced oxygen contamination and impurities detected in the bulk material [7, 9].

Growth of CdZnTe material has been technically achieved by the growth techniques including liquid phase epitaxy, vapor phase epitaxy, molecular beam epitaxy, and bulk growth methods. There exist various methods having different specialized names such as solvent evaporation, liquid encapsulated Czochralski, zone refining, solution growth, heat exchanger method, float-zoning, Bridgman, vertical gradient freeze, and traveling heater method [7, 12]. However, only last three of these methods stated above have received attention and they are still widely used in bulk growth of CZT. These three growth methods have been effective in minimizing the effect of difficulties encountered during the growth of CdTe material family such as low thermal conductivity, tendency to twin formation, stoichiometry control, Zinc distribution, tilts/rotations in the CZT lattice, and impurities [7]. Despite remarkable progress in alternative substrates to CZT has been recorded for recent years, high quality epitaxial layers can only be achieved with the CZT substrates that provide a lattice matched substrate for MCT-based device [12]. In this part, three most common growth techniques (Bridgman technique, traveling heater method, and vertical gradient freeze technique) are summarized.

### **2.3.1 Bridgman Technique**

In Bridgman technique, elemental starting charge (Cd, Zn, and Te) is loaded into the designed crucible system such as graphite/pyrolytic boron nitride (pBN) crucible encapsulated by silica ampoule [13]. Next, high temperature homogenization process takes place. At temperatures in excess of 1100°C, rocking step is followed in a homogenization furnace [14]. In multi-zone Bridgman furnace, required thermal profile and the translation speed are first needed to be determined and after the growth, determined cooling profile is followed in a controlled manner. Growth is accomplished by crystallization of the melt translated from hot zone through cold zone (Figure 2.3).

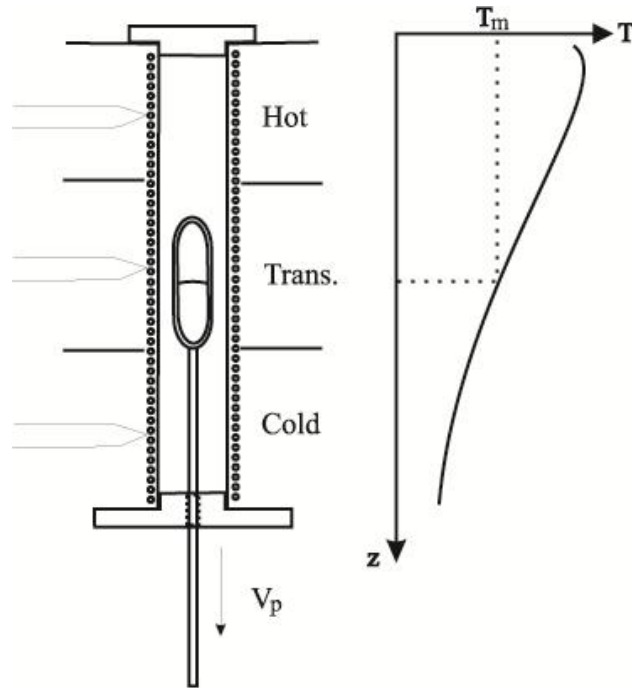


**Figure 2.3** Basic temperature fashion followed in Bridgman systems [26]

In order to improve the CZT growth using Bridgman technique, different varieties have been experimented. These include addition of excess Cd reservoir operating at a lower temperature, horizontal growth, vertical growth, low-pressure growth, and high-pressure growth [7]. Later on, more stable growths were achieved by the addition of the accelerated crucible rotation technique (ACRT) patented by Peter Capper in 1985 [15]. Bridgman technique came out with the earliest synthesis of CdTe and this technique is still used for the growth of CdZnTe by research groups and industry. Size, purity, stoichiometry, crystal quality, and crystal yield are major issues of Bridgman technique. In order to avoid or at least minimize these problems, Bridgman technique with overpressure control is mostly preferred [9].

### 2.3.2 Traveling Heater Method (THM)

In the last two decades, THM method have gained different names and terms such as ACRT, focused radiant heating, sublimation-THM, multipass THM, and cold THM by the variations on the basic applications of this technique itself [7]. Grown crystals are obtained either starting with elements (Cd, Zn, and Te) or pre-compound materials (CdTe or ZnTe). THM method was first developed by Robert Triboulet for the growth of Te-based II-VI materials [7]. Conventional CdZnTe growths are normally accomplished by the slow movement of the growth ampoule relative to the heater. The THM technique is based on the migration of a molten zone through the solid charge. During the growth of CdZnTe, homogenized solution of CZT is held molten by a narrow heater. As the heater moves up slowly, then the crystallization occurs at the growth interface [16]. THM process is shown in figure 2.4 schematically.

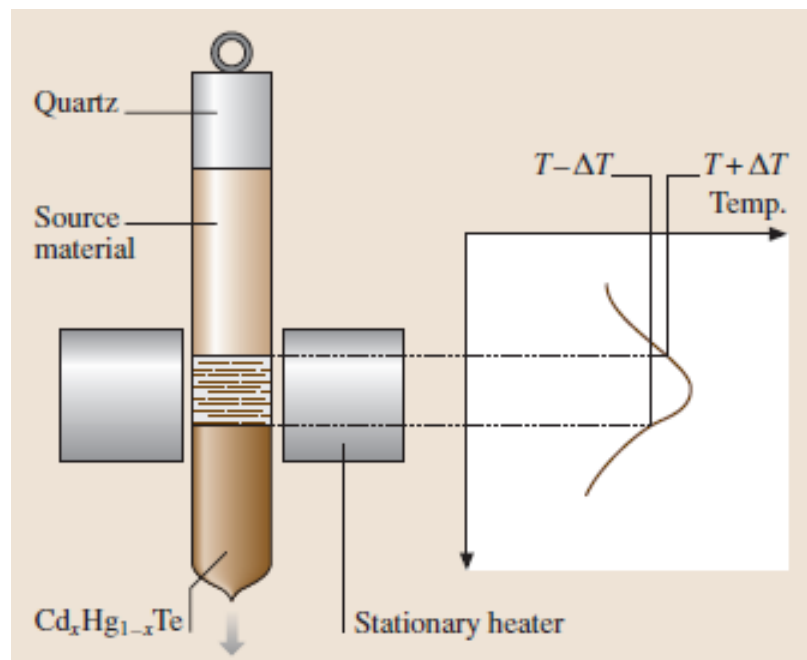


Figure 2.4 Schematic of THM method growth system [12]

In THM method, the vital point is to obtain the optimum temperature profile providing material transport by convection and diffusion through the molten zone [7].

### **2.3.3 Vertical Gradient Freeze (VGF)**

In vertical gradient freeze technique, the continuous freezing of the lower end of a melt upwards takes place. This freezing process can be controlled by two different fashions. For the freezing process, either the furnace can be moved to past the melt or, alternatively, temperature gradient throughout the furnace having independent temperature zones can be moved. Low-temperature gradients offer low dislocation density, defined crystal shape and size. However, difficulties in furnace design and the boat selection (crucible) are generally encountered [7, 12].

## **2.4 Experimental Details – Bulk Growth of CdZnTe in Three-Zone Vertical Bridgman Furnace**

This section introduces the experimental details of the bulk growth of CdZnTe material at METU. During this study eight growths have been performed. Growth parameters such as temperature profile and the pull rate were varied in order to obtain better crystal quality material. Each growth has been labeled as “CZT-X” where `X` is the growth number. About three ingots out of eight were chosen for sample preparation and characterization. Although there are differences in some parameters during the growths performed, a typical growth run includes the following steps:

- Crucible selection
- Ex situ cleaning of crucible and silica growth ampoule

- Preparation of starting charge
- Ampoule sealing
- Homogenization of starting charge
- Bridgman session and controlled cooling
- Growth end and obtaining CZT ingot

#### **2.4.1 Selection of Crucible Material**

Demand on high quality CZT substrates has pushed research groups and industrial manufacturers to study on crystal growths with reduced impurity. Contamination from the crucible during the growth is the primary impurity source [17, 18, 19, 20]. Therefore, selection of crucible material is of great importance prior to growth. In order to minimize the contamination, various types of crucibles such as quartz, carbon-coated quartz, graphite and pyrolytic boron nitride (pBN) are widely used for CZT crystal growth. Since the quartz is known to be the oxygen contamination source due to strong interaction between the crucible walls and the melt inside, graphite and pBN are mostly studied and their effects on the crystal quality are reported [21, 22]. Graphite crucibles are also known to be the source of carbon contamination. When graphite and pBN crucibles are compared in terms of crystal quality outcome, pBN is reported to offer slightly more advantages and pBN shows steeper thermal profile when compared to graphite. That is, when the heating zones of the furnace are set, steeper thermal profile indicates the less deviation from the temperatures set [23]. pBN, unique ceramic material, is of material advantages such as non-porous structure and it does not have any toxicity data. Moreover, its high purity, mechanical durability, and heat stability enable to be used in high temperature applications. pBN also shows inertness and stability at temperatures up to 850 °C in oxidizing atmospheres and up to 2800 °C in reducing atmospheres [24]. After all these comparisons and the reasons stated above, pBN was selected as a crucible material for growth studies conducted at METU.

## 2.4.2 Designs of Silica Growth Ampoule and pBN Crucible

As stated previously, growth method and followed steps were determined according to the availability of the systems, instruments, and growth infrastructure. Initially, three-zone vertical Bridgman furnace, located at METU Physics Department, was tested to check for the conformity to the required temperature and translation parameters for CZT growth. Mainly, Bridgman furnace is of three independent heating zones and each zone is about 150mm. Although its bore diameter is specified as 50mm, the ampoule support allows only up to 20mm-diameter growth ampoules. The furnace can be set to a maximum temperature value of 1200 °C and it is of a total translation length of 300mm. Translation can be adjusted between 0.001 and 999.9 in units either mm/h or mm/min.

Taking into account all these constraints and required parameters for CZT crystal growth, first, pBN crucibles were designed as show in figure 2.5.

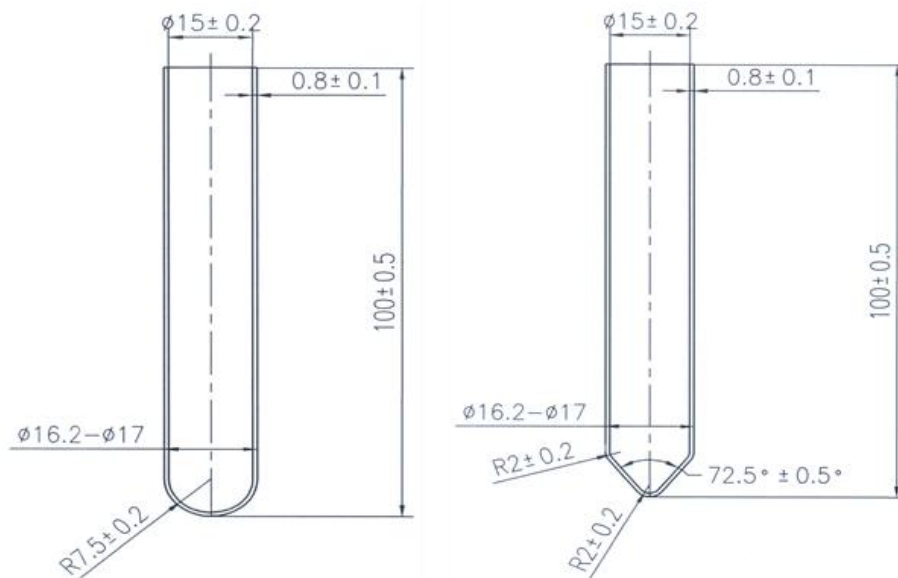


**Figure 2.5** Technical drawings of pBN crucibles designed at METU

In order to compare the tip effect on the crystal quality, additional designs were formed including crucibles having tip region (Figure 2.6).

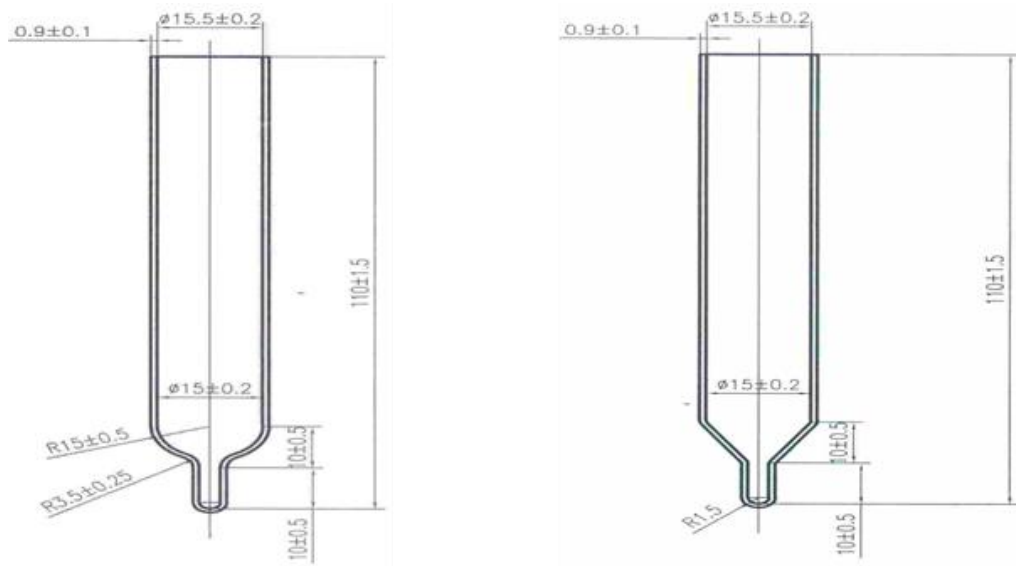


**Figure 2.6** Technical drawings of pBN crucibles designed at METU  
(a) Rounded shape crucible with tip region, (b) V-shaped crucible with tip region

It was reported that tapered tip region induces nucleation centers in the corner of the crucible where the temperature is minimum and facilitates the self-seeding phenomenon [7]. After specifying the designs of pBN crucibles, quartz growth ampoules were designed as shown in figure 2.7. Finally, quartz ampoules and pBN crucibles were manufactured, and pBN crucibles were placed into the ampoules. Quartz growth ampoules are required for ampoule sealing in low-pressure Bridgman technique.

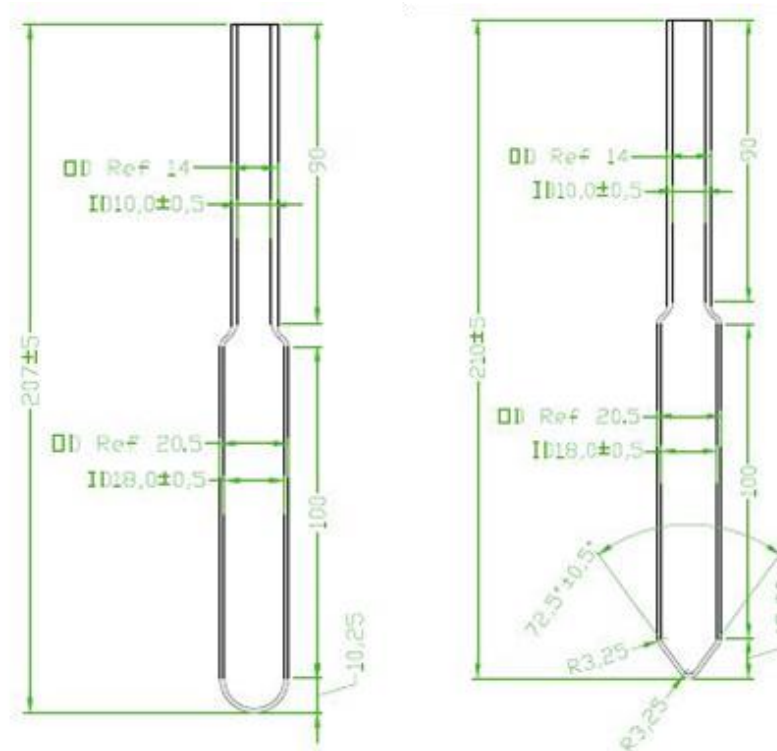


**Figure 2.7** Designed silica growth ampoules used for sealing prior to growth  
 (a) Rounded shape quartz ampoule, (b) V-shaped quartz ampoule

### 2.4.3 Preparation and Homogenization of Starting Charge

This study aimed at obtaining single crystal regions having (211) crystal orientation from CZT boules to be grown. After determining the single crystal regions, thin slices are obtained from this region and tested for a series of substrate characteristics in order to specify their quality. As a starting material preparation, for  $\text{Cd}_{1-x}\text{Zn}_x\text{Te}$  ( $x=0.04$ ), elemental form of Cd, Zn, and Te with high purity (7N, 99.99999%) were weighed, then loaded into the pBN crucible/quartz ampoule system under clean room conditions to avoid potential impurities. The amount of charge varied between 20-30 grams, constrained by the ampoule and furnace dimensions. Next, quartz ampoule was sealed at a relatively low pressure about  $2 \times 10^{-5}$  Torr.

Prior to the homogenization process, a horizontal furnace having single heating zone was modified; so that it could be used in vertical operation. Besides, a home-made rocking apparatus was developed (Figure 2.8).



**Figure 2.8** Vertical homogenization furnace with rocking apparatus located at METU Physics Department

Sealed ampoule of starting charge is placed into the quartz tube/ampoule holder hanged by the use of heat resistive kanthal wires from the top end cap made of quartz. The hanging position of the starting charge corresponds to exactly the middle of the furnace where the temperature distribution is known to be homogeneous. Lower end of the furnace is closed by an alumina end cap. All these system

components have been designed at METU. Sealed growth ampoule having starting charge in it is now ready for the heat treatment of homogenization process. The accumulated experience after each growth optimized the homogenization of starting charge. During the homogenization, we paid special attention to both heating rate and cooling rate. Homogenization was performed with the temperatures and times specified in table 2.1.

**Table 2.1.** Temperatures and times followed during the homogenization process

Temperature (°C)	Elapsed time (hour)	Notes	Cooling profile (°C)	Elapsed time (hour)
200	½	-	1200	-
300	½	-		
321	½	Cd (M.P.)	1100	1
420	½	Zn (M.P.)	1000	½
452	½	Te (M.P.)	800	½
500	1	-	700	1
600	1	-		
700	1	-	600	1
750	1	-	500	1
800	1	-	400	1
900	1	-	300	½
1000	1	-	200	½
1100	15	-	100	½
1200	6 (rocking)	(rocking)	Room temperature	-

Since the homogenization furnace is not equipped with a programmable temperature controller, each new entry for the temperature setting should be done manually by hand. Indeed, this prevented applying smooth, low temperature gradient profile to the starting charge. Cooling down process could be performed also in an uncontrolled manner. Each homogenization session of starting charge lasted about 40 hours.

In the end of the homogenization, growth ampoule was inspected by unaided eye whether there formed an abnormal situation such as ampoule breakage or cracking.

Following to the inspection and checking of the growth ampoule, Bridgman session took place to finalize the CZT crystal growth.

#### 2.4.4 Bridgman Session of CdZnTe Crystal Growth

For Bridgman session of CZT crystal growth in three-zone vertical Bridgman furnace, we need to determine growth parameters such as independent zone temperatures and translation speed and direction. On the main control unit of the furnace (Figure 2.9), these parameters are set prior to growth.



**Figure 2.9** Three-zone vertical Bridgman furnace located at METU Physics Department

Different zone temperatures and thermal profiles have been tried, and the optimum zone temperatures of the furnace were found to be 1150 °C, 950 °C, and 800 °C, from top to down, respectively. Lower thermal profiles were observed to have serious negative effects on the crystallinity and led to the CZT ingots having porous structure.

Since the translation should be performed from hot zone to the cold zone, translation direction was from up to down, and translation speed was determined to be 2mm/h.

During the Bridgman session, first, the furnace was set to the zone temperatures as stated above. Once the zone temperatures reached the set values, intended temperature profile was followed carefully to check whether there was any temperature deviation. After being sure that zone temperatures were stable, then the translation was initialized. Active translation length is about 180mm and translation finished automatically after 90 hours with a speed of 2mm/h.

Following the translation, the ingot was cooled down to room temperature with a cooling rate about 50 °C/h, manually. Cooling down process lasted about a day and after the CZT crystal growth was finished, growth ampoule was taken out from the furnace. The ampoule was broken by a small hammer or cut using a diamond cutter. The latter is preferred when a pBN crucible is used inside the quartz growth ampoule because pBN crucibles are generally used for at least more than one growth, so the care must be taken to avoid breakage or delamination. When pBN crucible is used, CZT ingot probably slips from the pBN crucible due to the small interaction of each other. Once the CZT ingot is obtained, then it is inspected via unaided eye and optical microscope prior to slicing operation.

## **2.5 Conclusions**

Throughout this chapter, CZT properties related to the bulk growth process have been presented. As a structural property, lattice-match between CdZnTe substrates and HgCdTe epilayers has been emphasized. Phase diagrams of CdTe and CdZnTe

have been given as thermal properties. Next, widely used growth techniques have been given, briefly.

In the experimental part, growth details such as crucible selection, charge preparation, homogenization and crystal growth have been provided, explicitly. Different designs of pBN crucibles were used in growth trials; nevertheless, it was not possible to conclude the effect of crucible shape on the ingot's crystal quality. This is considered as due to the thermal instability in the furnace and lack of quality in isolating regions between so-called independent isolated heating zones.

## **CHAPTER III**

### **CADMIUM ZINC TELLURIDE WAFER PROCESSING**

#### **3.1 Introduction**

In addition to the electrical, optical, and structural constraints and demands, advanced MBE growth technology of HgCdTe epilayers requires CdZnTe substrates with superior physical properties such as surface roughness, thickness variation, and orientation accuracy [9]. Therefore, CdZnTe wafer processing is of high prominence for obtaining desired high-quality surfaces to perform epitaxial growth of HgCdTe, successfully. Studies on epi-ready-like substrates for MBE growth are being conducted intensively by semiconductor manufacturers and defense industry. This chapter includes main wafer processing steps based on state-of-the-art technology followed by research groups. As experimental studies, wafer processing steps optimized at METU were also included in each section.

#### **Flow Steps of CdZnTe Wafer Processing**

Before starting to discuss each process, separately, it is more convenient to have a look at the overview of general wafer processing of CdZnTe as shown in figure 3.1.

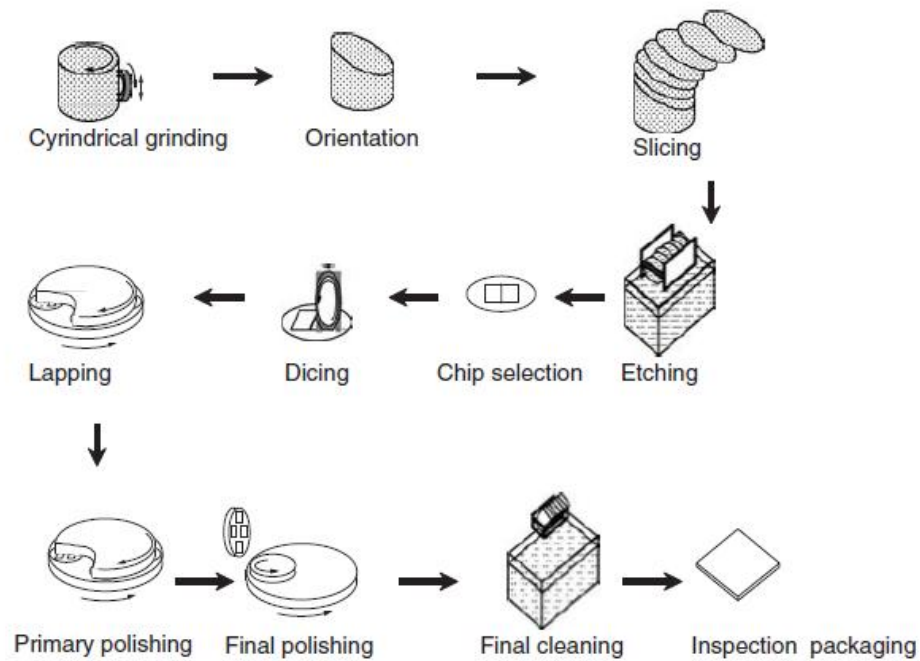


**Figure 3.1** Schematic flow of CdZnTe wafer processing [9]

### 3.2 Ingot Slicing

After cylindrical grinding, the end of the CZT crystal is cut using annular saw, corresponding to the orientations  $\langle 111 \rangle$  and  $\langle 211 \rangle$ . For the growth of MCT epilayers, these two specific orientations are vital for the LPE and MBE, respectively. If the crystal's growth direction is in  $\langle 111 \rangle$ , then in order to obtain (211) face, CZT ingot is cut diagonally. Once the desired slice is acquired (i.e. end cutting), multi-cut process is followed to obtain slices parallel to the end face, which is (211). For industrial mass production of CZT wafers, multi-wire saws are widely used in slicing of CZT ingots as for the Si ingots. Multi-wire saws offer reduced slicing damage and minimum kerf loss, which is the amount of material loss during a cutting process and is highly crucial in determining the cost in manufacturing

process. In 2011, slice cutting of 5-in diameter CZT ingots were reported to be accomplished [9].

Up to 0.7-in diameter CZT ingots grown at METU were sliced to obtain 5mmx5mm single crystal wafers. Grown ingots were cut using two different cutting instruments including Struers Accutom-50 annular saw and IBS Grafrath WSB 22 wire saw. Former offers multi-cuts in a short time interval; however, both kerf loss and slicing damage is higher. Conversely, the latter offers low kerf loss and reduced slicing damage, but the cutting speed is extremely slower ( $\sim 0.3 \text{ cm}^2/\text{h}$ ).

In studies conducted at METU, both two cutting instruments were used according to the desired application. While the tip region of the grown CZT ingot was cut using annular saw, desired slices were obtained using wire saw in order to avoid possible breakage of the ingot due to relatively higher force applied by the blades. For annular saw case, diamond coated steel and SiC blades were used to separate the tip region from the ingot itself. Slicing trials were also performed and it was observed that for slices having thickness larger than about 2mm, cutting was successful. However, for substrate grade CZT, the desired thickness should be around 800 $\mu\text{m}$ . This thickness value could be accomplished by grinding, but material loss would be much higher. More than half of the slice in terms of thickness would be recorded as material loss, which causes low yield from each ingot. When the blade types are compared, diamond blade offers more stable cuts and end surface after the cut is of better quality. Since the diamond blade is thicker (800 $\mu\text{m}$ ) than the SiC (500 $\mu\text{m}$ ) blade, fairly thicker slices can be obtained due to groove size formed on the ingot during the cutting process. SiC blade offers relatively thin slices, but serious cracks of ingots were observed.

After separating the tip region of the ingot, slices perpendicular and parallel to the growth direction were obtained using wire saw. Since the kerf loss and slicing damage are much lower in the wire cutter case, down to 1mm-thick slices were obtained. Acquiring thinner slices is also possible down to 500 $\mu\text{m}$ , but note that the thinner the slices are, the more fragile the substrates are. Typical slicing session involves the following steps: First, the ingot is mounted on a holder of the wire saw using wax (in annular saw, mounting is done by screws). Next, the ingot is aligned

for the intended slicing. For the ease of cut, cutting liquid is prepared prior to each cut. This is prepared manually in a dedicated container attached on the wire cutter. Cutting liquid is composed of volumetric mixture glycerine:SiC powder (10:1).

Following the alignment of the ingot for the desired slice (i.e. thickness and end cutting position), the slicing is initialized. Precision slicing is accomplished via tungsten wire having diameters of 40 $\mu$ m, 50 $\mu$ m, 60 $\mu$ m. Precision of slices depends on the alignment of the wire cutter system and tension of the wire. Each slicing process prolonged about more than 7 hours. This elapsed time is strongly dependent on the material itself. For CZT ingots having porous structure, cutting time will be shorter as expected. Conversely, in the case of CZT ingots having good quality and solid structure, slicing times lasting overnight have been experienced.

The primary aim of these CZT studies was to obtain single crystal CZT having dimensions 5mmx5mm and  $\langle 211 \rangle$  crystal orientation. In accordance with this aim, initially, ingots were sliced either perpendicular or parallel to the growth direction in somewhat randomized fashion. Since the grown ingots are of much smaller volumes than the industrial ones, industrial cutting methods are not so feasible.

### **3.3 Lapping**

Lapping is a crucial process of wafer processing because, as previously stated, the thickness variation throughout the CZT wafer is critical for epitaxial growth of MCT. Even if all difficulties or problems encountered during the growth of larger diameter CZT substrates were avoided, especially for large-scale CZT substrates, total thickness variation (TTV) would still be a major problem in successful device processing. Thickness variation is minimized or even avoided by the lapping process. Once this process is optimized, thickness variation from wafer to wafer is reduced and flatness on each wafer is seriously improved. Optimized lapping process involves double-side lapping rather than single-side lapping [9].

CZT slices obtained from the grown ingots at METU were grinded into desired thickness values. 1mm-thick slices were lapped until 800 $\mu$ m-thickness value

obtained using several lapping films attached on the polishing machine. 1mm-thick slices were first grinded down to 850-900  $\mu\text{m}$  and then lapped down to 800 $\mu\text{m}$ .

The whole lapping process was performed using Allied High-Tech MultiPrep lapping and polishing system. Alignment of lapping and polishing system is performed prior to each lapping session. TTV value of parallel polishing fixture is checked by using Mitutoyo Magnetic Base. CZT slice to be lapped is mounted on the parallel polishing fixture using wax. Next, diamond lapping films are attached on the metal lapping plates. Lapping films are of different particle sizes including 35-30-15-9-6-3-1-0.5-0.25-0.1  $\mu\text{m}$  (Embedded diamond particles into plastic films). These films are used successively starting from the largest size film. During the lapping process, the total amount of material loss varies between 150-250  $\mu\text{m}$ , depending on the initial thickness and surface quality. The total amount of material removed for each lapping film was specified below (Table 3.1), and acceptable TTV values (<40 $\mu\text{m}$ ) were reached as initial studies.

**Table 3.1** Size of diamond particles in lapping films used and the total amount of CZT material removed

Diamond film particle size ( $\mu\text{m}$ )	The amount of material removed ( $\mu\text{m}$ )
35	100*
30	52.5
15	45
9	22.5
6	13.5
3	9
1	4.5
0.5	1.5
0.25	0.75
0.1	0.375
Total: $\sim 250\mu\text{m}$ , * Initial amount of material removed, determining the total amount.	

### 3.4 Grain Revealing and Dicing

Slices cut from grown CZT ingots were subjected to bromine-methanol ( $\text{Br}_2\text{-MeOH}$ ) etchant to remove slicing damage. Other reliable etch solutions such as Nakagawa, Inoue, and Everson are used for the revealing of dislocations and microtwins depending on the crystal orientation since the etchants are strongly orientation dependent. After etching, usable single crystal area on the CZT slice is marked out, and single crystalline areas are singled out as rectangles or squares by using proper dicer. Dicer blade selection is of great importance due to fragile structure of CZT slices since these are easily chipped during the dicing process. Therefore, dicing

blade with proper bonding type should be determined prior to the dicing process. Besides, mechanical dicing conditions such as blade rotation and table speed are other prominent parameters requiring special attention.

Dicing processes of CZT slices grown were performed using Disco ASD111 dicer. Determined single crystal areas were cut along the lines to obtain the largest single crystal piece from the processed slice. These obtained single crystalline pieces were processed further for electrical, optical, and structural characterization.

### 3.5 Lapping and Mechanical Polishing

Obtained single crystalline CZT pieces are lapped again to avoid the morphological defects after etching. Following the extended lapping process, CdZnTe substrates are subjected to two main polishing steps. Primary polishing is the obtaining mirror-like surfaces using colloidal silica and hard pads or glasses for stock removal. Final polishing involves the fine polish with porous polishing cloths [9].

Home-grown CZT slices were subjected to both primary and final polishing for further surface finishing processes and characterization. As a primary polishing, various sizes of lapping films provided mirror-like surfaces and diamond particle embedded plastic lapping films acted as hard pads (Figure 3.2).



**Figure 3.2** Diamond lapping films and microscope image of diamond particles

Next, as a final polishing, final silk polishing cloth was used with colloidal silica suspension (40nm diameter SiO<sub>2</sub> nanospheres). This suspension is normally used for final polishing of Si wafers. It is reported that colloidal silica suspension is not feasible for polishing compound semiconductors such as GaAs and CdZnTe due to their fragility. Although chance of breakage is low during the final polishing, but the use of colloidal or powdered silica scratches and damages CdZnTe wafer surface with an immediate effect. To avoid this, bromine-methanol is widely used as a chemical polishing solution for almost all III-V and II-VI material systems including CdZnTe [9]. Nevertheless, recent studies have shown that bromine-methanol is not reproducible from time to time and orange-peel-like surface morphology is observed on CZT wafers [25]. Throughout the studies at METU, reproducibility problem of bromine-methanol usage and orange-peel-like surfaces have been experienced. However, chemical polishing procedures have not been performed due to weakness of polishing machine against bromine [9]. Alternatively, chemical etching in bromine-methanol was followed and the details of this process are given in the following section (3.6 Chemical Etching).

### **3.6 Chemical Etching**

Since bromine-methanol is highly corrosive, during the chemical polishing process, polishing machine is affected by bromine-methanol solution in time and its life is shortened. In CZT studies at METU, chemical etching was performed alternative to the chemical polishing due to the possible corrosion of polishing machinery. Chemical etching with bromine methanol was performed by dipping CZT wafers into the bromine-methanol solutions having bromine concentrations between 0.5 to 2 percent for up to 2 minutes. It was observed that slicing and lapping damages were removed after chemical etching. While some of the wafers had clean and high quality surfaces, a few of them had deteriorated and blurred surfaces. This may be due to the bromine exposure time of CZT wafers and problems in reproducibility. Good quality

surfaces were obtained after chemical etching so that these CZT wafers were used for EBSD analysis, which indicates the good surfaces.

### **3.7 Inspection**

Total thickness and total thickness variation of each CZT wafer are measured following the polishing process. After surface finishing steps, CZT wafers are inspected with both unaided eye and microscope to view defects and surface problems. CZT wafers produced were inspected using optical microscope and SEM.

## CHAPTER IV

# CADMIUM ZINC TELLURIDE CHARACTERISTICS AS SUBSTRATES FOR THE EPITAXIAL GROWTH OF MERCURY CADMIUM TELLURIDE

### 4.1 Introduction

As emphasized previously, quality of MCT epilayers is the key factor determining the performance of MCT-based IR photodetectors. High quality and successful growth of MCT epilayers requires high quality and lattice-matched substrates. Although growth studies on alternative substrates are being conducted, CdZnTe is still the primary material for epitaxial substrates [9]. However, due to difficulties encountered during the growth of CdZnTe and high manufacturing cost, high quality CdZnTe material is grown by only a few research centers and defense companies. The term “high quality” is defined by the superior optical, electrical, structural, and physical specifications. This chapter presents these desired characteristics that make CdZnTe substrates “high quality”.

### 4.2 Purity, Inclusions, and Precipitates in CdZnTe

CdZnTe substrates are produced by either conventional or state-of-the-art approaches. It is reported that growth from liquid phase (i.e. melt growth of CZT

material) is known to produce higher single crystal yield [7]. Typical growths using melt growth techniques, described in Chapter 2, barely produce epi-ready substrates due to the existence of structural defects. Dislocations and twins are counted as crucial defects in CZT ingots in which they are formed during the crystallization and cooling process [26-29]. Apparently, these defects in the CZT substrates cause instability in the structural quality and degrade the device performance of MCT-based IR photodetectors fabricated upon it. Other than these defects stated above, secondary phases are also known as defects in the CZT crystals and their size and shapes are influenced by the growth parameters and processes [30]. These are micro-scale defects that are being widely studied by different characterization techniques such as IR imaging, SEM, TEM, SEM/EDX, and Auger spectroscopy [7]. While the first three of these are for structural analysis, the last two techniques are for the compositional analysis. In CdZnTe wafers, micro-scale secondary phases are determined as Te or Cd inclusion and precipitates formed during the crystal growth [9]. Although the terms ‘inclusion’ and ‘precipitate’ seem very similar to each other, indeed, they differs in terms of size and formation mode. That is, inclusions are bigger in size than precipitates. Impurities in CZT substrates originate from the various sources. Some of the impurities are due to starting materials (Cd, Zn, and Te), and some others result from the containers and crucibles used during the crystal growth [7, 23]. When these two types of impurity sources are taken into account, the latter type of impurity source can be counted as the main impurity source since the starting materials are extremely pure (7N purity grade). These impurities disperse throughout the substrate and during the epitaxial growth of MCT layers, impurities in the substrates diffuse out into the epi-layers [9]. This impurity diffusion phenomenon degrades the electronic properties and device performance of MCT epilayers. Impurity-associated dislocations also serve as channels for Hg diffusion from the epi-layer to the CZT substrate [9, 26].

Since these secondary-phase impurities in CZT substrates cause dramatic degrading effects on the performance of MCT-based IR devices, serious amount of work have been conducted in order to avoid or at least minimize these impurities [27]. As a post growth processing, annealing (thermomigration) is generally performed to reduce secondary phases formed during the crystal growth. In this thermomigration process,

it is reported that either Cadmium or Zinc is used as annealing source and the annealing source temperature is kept at a lower temperature value than the CZT substrate temperature. Across the CZT substrates, a temperature gradient is applied to enable the thermal migration of secondary phases as a driving force. For the reduction of Te secondary phases, CZT substrates are maintained at a temperature above Tellurium's melting point. In this case, Te secondary phases migrate from the cold to the hot side of the CZT wafer [28].

In addition to post growth processing of CZT wafers, there exists a widely accepted technique for the growth of CdZnTe substrates which are free from the secondary phase impurities. This technique is based on the in situ control of secondary phases during the crystal growth and can be adapted to the various growth methods. Specifically, in this technique, formation of secondary phase Te particles are controlled by saturating the vapor phase over the melt with the most volatile material [11]. Here, this material is Cadmium and it is of the lowest boiling point (Cd: 767 °C, Zn: 907 °C, and Te: 988 °C). This process, dynamic control of vapor pressure, is performed using an extra Cd source in a separated reservoir placed in the silica growth ampoule. Another alternative way of controlling vapor pressure is suggested by addition of excess Cd into the starting charge. The required amount of excess Cd is determined as a function of corresponding vapor pressure, the free volume over the melt in a growth ampoule, and the melt temperature [11, 12].

### **4.3 Zn Distribution in CdZnTe Wafers**

Another key requirement for CZT substrates is the homogeneity of Zn concentration throughout the surface of the wafer. Large-area CZT substrates are required for the epitaxial growth of large-area and homogeneously lattice-matched HgCdTe. High demands to large-area requirements are for the manufacturing of larger IR focal plane arrays. Since the lattice constant in  $\text{Cd}_{1-x}\text{Zn}_x\text{Te}$  (where  $x=0.04$ ) is strongly dependent on the  $x$  value, for the epitaxial growth of homogeneously lattice-matched MCT, CZT substrates should have homogeneous Zn concentration throughout their surfaces as well as required Zn concentration (4%) [9]. Zn distribution throughout

the CZT ingots and wafers is known to vary. After crystal growth, CZT boules are sliced and these CZT slices are subjected to a series of wafer processing steps described in Chapter 3. As a part of characterization, CZT wafers are required to have homogeneous Zn distribution. Post growth annealing of CZT crystals is observed to increase the homogeneity of Zn distribution. Different annealing temperatures and time are tried by various research groups. For instance, the Zn concentration of a CZT crystal differs only within 1% around the 40% of the crystal in size. Then, following the post growth annealing, a prolonged annealing for 10 days at 1000 °C and cooling with rate of 10 °C/h to room temperature, around 75% of crystal in size is of Zn distribution variation within 1%. These post growth annealing processes reduce the variation of Zn distribution by the solid state diffusion of Zn [29].

#### **4.4 Infrared Transmission**

In general, optical transmission of semiconductor wafers are directly related to the crystalline imperfections. For CdZnTe case, Te precipitates are the primary factor degrading the IR transmission of CZT wafers. It is considered that at shorter wavelengths, IR light extinction is dominated due to scattering of precipitates; whereas, at higher wavelengths, it is dominated by the free carrier absorption. It is obvious that IR transmission increases with decreasing carrier concentration (Figure 4.1 (a)) [9].

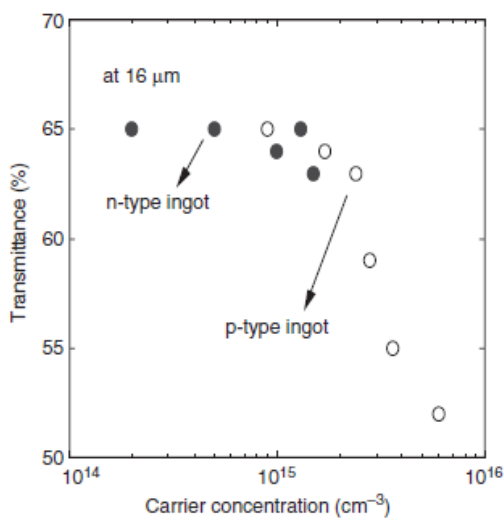
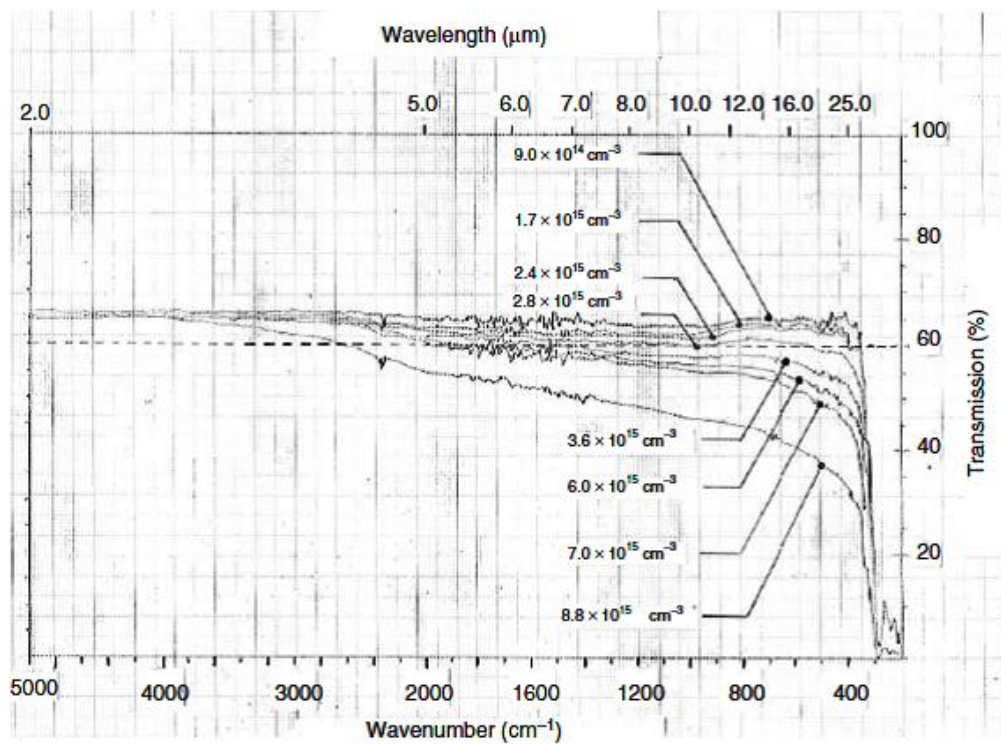


**Figure 4. 1** (a) Carrier concentration dependence on IR transmission of CZT crystals, (b) Carrier concentration dependence on IR transmission of p-type and n-type ingots [9]

While Tellurium-rich CdZnTe ingots show p-type behavior, Cadmium-rich ingots are n-type. In Figure 4.1 (b), n-type ingot is of higher IR transmission due to lower carrier concentration [7]. Since the imperfections and impurities in CZT crystals are the main factors affecting the IR transmission, these defects should be avoided or at least minimized. IR transmission of CZT crystals increases by reducing Te precipitates that are known to degrade the optical transmission. This is accomplished by post growth annealing of CZT crystals. It is reported that annealing at 800-900 °C under Cd or Zn vapors, reduced the secondary phases and IR transmission increased [30]. Moreover, after annealing, dramatic increases were observed in IR transmission of even nonstoichiometric CZT wafers. However, post growth annealing process does not always lead to higher optical transmission values. Some CZT wafers were reported to have lower IR transmission (IRT) even after the annealing processes. Although the carrier concentration gets lower following the annealing process, this may not have enough to increase the transmission. It is also required to reduce Te precipitates to observe an increase in IRT [31]. Both precipitate density and carrier concentration should be taken into account for the investigation of IRT. Te precipitates get smaller, gradually during the annealing; nevertheless, initially, free carrier concentration becomes higher locally around the precipitates, but then the concentration become smaller following the disappearance of precipitates [12]. Therefore, longer annealing times is more preferable. Commercial CdZnTe wafers having thickness of 800 $\mu$ m are of transmission values are around 60% and more for the wavelength interval 2-20  $\mu$ m [9].

## **4.5 Crystallographic Surface Orientation**

Substrate surface orientation is crucial for the HgCdTe epilayers growth in MBE. In order to grow high quality (i.e. low dislocation and strain free) MCT epilayers, it is extremely important to match the lattice parameter of the substrate. This is the fundamental rule for the epitaxial growth. This was recognized during the early studies of HgCdTe growth on CdTe substrates. It is known that sticking coefficient of Hg shows strong dependence on the substrate orientation [9]. Besides, epitaxial quality of MCT is also dependent on orientation. Briefly, first MBE growths of MCT

material were performed on CdTe substrates having low-index planes such as (100) and (111). However, these planes were reported to induce microtwinning in epilayers. Later it was understood that the epitaxial growth on (211)B substrates yield a high quality surface morphology, suppression of twinning, higher Hg sticking coefficient, and better control of composition [9, 12]. Today almost all MCT growths are being carried out on (211) CZT substrates. In notation “(211)B”, ‘B’ denotes the crystal polarity (i.e. anion-rich substrate surface), which is discussed in Section 4.7 in detail.

## **4.6 X-ray FWHM and Crystallographic Misorientation**

Since the crystal quality and crystallographic misorientation (orientation accuracy) of CdZnTe substrates are very important for the epitaxial growth of HgCdTe, the X-ray analysis is extensively used for the crystal characterization. It is also very useful to correlate the X-ray data with the average etch pit density (EPD) to understand the crystal quality. A brief description of the X-ray analysis is given below.

### **4.6.1 X-ray FWHM**

X-ray FWHM (Full width at half maximum) value is a useful parameter indicating the quality of the crystal. In general, FWHM is used to describe a measurement of the width of a curve having no sharp edges [32] (Figure 4.2).

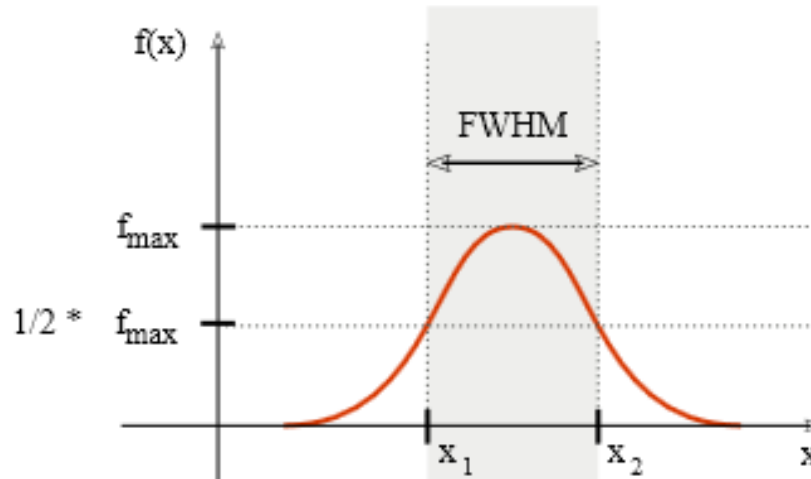


**Figure 4. 2** Schematic of a general FWHM concept [38]

When MCT epilayers are grown on low crystal quality CZT substrates, it is observed that MCT epilayers exactly show the same defect map of these substrates. Twins, grain boundaries, and other surface defects are repeated in the epilayers. In order to avoid these types of defects in MCT epilayers, it is highly prominent to use high quality CZT substrates. The crystal quality of the CZT substrate is measured by the X-ray rocking curve measurements from which FWHM value is determined. Narrower peak widths (i.e. smaller FWHM values) indicate better crystal quality. Defects and impurities in CZT wafers contribute to the X-ray signal and cause peak broadening. In this case, FWHM values are higher. Desired crystal quality (i.e. FWHM value) may vary depending on the application; however, commercial, high quality CdZnTe substrates are of FWHM values below 20 arcsec and CZT crystals grown by state-of-the-art growth methods are of even below 10 arcsec FWHM values.

#### 4.6.2 Crystallographic Misorientation

In addition to structural and physical requirements of CZT substrates for MCT epitaxy, crystallographic misorientation, affecting the morphology of epitaxial layers, is also necessary. Crystallographic misorientation can be defined as the angular deviation in the surface orientation relative to the intended surface orientation. Technically, CZT wafers having minimum misorientation or even accurately oriented CZT wafers can be obtained by properly performing ingot slicing process (i.e. end-cutting). Specifically, the end cutting process is so critical because the successive multi-cut process repeats the surface obtained after the end cutting process [9]. That is, all slices will have the same misorientation as the end-cut surface. For the accurately oriented CZT wafers, it is extremely critical to adjust the oriented end face of the CZT ingot parallel to the cutting face (i.e. blade of annular saw). Stability of the blade during the cutting process also plays a key role in accurate slicing. Orientation accuracy value about less than  $0.1^\circ$  is achievable by state-of-the-art cutting methods [9].

#### 4.7 Polarity Determination of CZT Wafers

Crystallographic polarity of CdTe substrate family is of great importance for HgCdTe epitaxial growth and specialized chemical etching processes. Specifically, as stated previously, CdZnTe substrates with (211) faces and having polarity B, (211)B wafers, are commonly preferred for HgCdTe epitaxy in MBE reactor. This crystallographic polarity is based on the crystallographic structure of CdZnTe material. Polarity refers to the difference of structural and chemical properties of opposing crystal planes such as (hkl) and  $(\bar{h}\bar{k}\bar{l})$ . For grown CdZnTe ingots, following the slicing process, it is known that while one side of the slice is A face, the opposite side of the slice is B face. This is the case for {111} faces. In other words, when the crystal growth direction is  $\langle 111 \rangle$ , and if one obtains a slice perpendicular to the growth direction, then one side of the slice is of A polarity and the other side of the slice is of B polarity. Labeling of A and B polarities, which is done by convention, refers to the following: The {111} surfaces are Cadmium-terminated surfaces and

labeled as 'A'. Conversely, the  $\{\bar{1}\bar{1}\bar{1}\}$  surfaces are Tellurium-terminated surfaces and labeled as 'B' [11] (Figure 4.3).

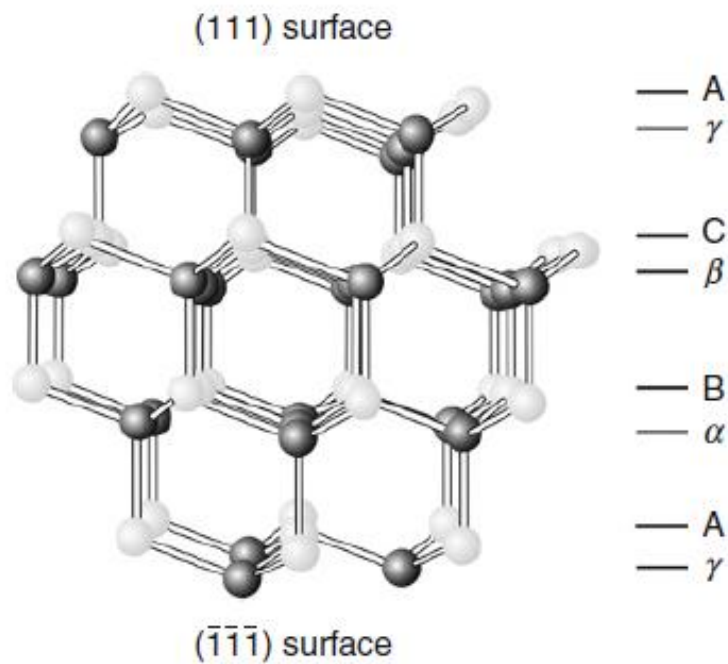


**Figure 4. 3** Cd-terminated and Te-terminated surfaces in CdTe structure [11]

Many attempts and studies including X-ray/etching method were conducted to determine the polarity of CdZnTe crystals. Fewster and Whiffin applied a new etchant in order to determine the crystal polarity of CdTe [33]. It was reported that in contradiction to the previously published work [34], after etching, pits formed on the A face (Cd-terminated), not on the B face (Te-terminated). Their results agreed with the other work [11]. Due to its importance in epitaxial growth, it is essential to optimize an accepted procedure determining the crystallographic polarity. In accordance with this purpose, in 1989, Brown et al. [35] reported upon the use of

alternative etchants to the previously used ones to develop more practical and efficient method for polarity determination. It is based on the use of HF:HNO<sub>3</sub>:acetic acid (1:1:1 v) and HF:HNO<sub>3</sub>:lactic acid (1:1:1 v) as polarity determining etchants. Both these two etchants yield a matt black surface on (111)A (i.e. Cd-rich) and a bright shiny surface on ( $\bar{1}\bar{1}\bar{1}$ )B (i.e. Te-rich) surface. Best results were obtained when the immediate water rinse was followed to etching process. This instant and efficient way of determining crystal polarity of CdTe substrate family can be applied locally as a liquid drop to the CZT slices so that the surfaces are not deteriorated by the etchants [11]. Another advantage of using Brown's polarity determination method is the direct observation of contrast difference on substrate surfaces by unaided eye.

#### **4.8 Etch-Pit Density (EPD) Measurements of CdZnTe Substrates**

Group II-VI compounds, CdTe and CdZnTe crystals contain precipitates, twins, dislocations, and low angle grain boundaries [7, 33, 36]. As described previously, X-ray FWHM is used to understand the crystal quality in general. In addition, etch-pit density measurement is commonly used and compared with the X-ray data to assess the substrate quality. Etch-pit density measurement is based on determining the number of pits formed on the substrate surface after a selective etching process. Pits on the selected area of a substrate are counted and the number of pits is extrapolated to the unit area (i.e. # of pits/cm<sup>2</sup>) using optical or electron microscopy.

For the defect etching studies, many defect etching approaches were developed by Inoue, Nakagawa, Bagai, Chen, Everson, Hahnert and Schenk [7]. Some of them are widely used methods; however, the accuracy and reliability of these methods are still being questioned. Therefore, these methods should be confirmed and supported by other characterization techniques. Although the effectiveness of these etching methods is still controversial, either Everson or Nakagawa etch is often applied to the CZT substrates to reveal dislocations and precipitates. While Nakagawa etch is used for (111)A surface etching [34], Everson etch is used for the etching of (111)B and

(211)B surfaces [37]. For MCT-based detector applications, CZT substrates are required to have EPD values around  $10^4 \text{ cm}^{-2}$  [9].

## **4.9 Resistivity of CdZnTe Substrates**

MCT-based IR device performance is strongly affected by the average EPD and resistivity of CdZnTe substrates. For the epitaxial growth of mercury cadmium telluride, CZT substrates (undoped) having at least  $10^3 \text{ }\Omega\text{cm}$  are used. Similar to impurity case, the electrical properties of CZT substrates influence the grown MCT epitaxial layers. Low resistivity in the substrate creates electrical disturbances in the MCT layer grown upon it. This leads to a lower RA value that is crucially important for the detectivity of the photodiode [38].

## **4.10 Surface Roughness and Surface Oxidation of CdZnTe Wafers**

### **4.10.1 Surface Roughness**

The morphological quality of HgCdTe epitaxial layers is affected by the surface roughness of CdZnTe substrates. Research groups and companies in defense industry develop their own unique surface finishing chemical solutions most of which are of undisclosed chemical content. Nanometer-sized alumina suspension and colloidal silica suspension can be used; however, these were reported to cause scratches and other surface deteriorations due to fragility and softness of CZT material [9]. For surface roughness, there is not a minimum acceptable requirement as a parameter for the epitaxial growth since the substrate surface is required to be as perfect as it can be. Nevertheless, to have an idea about the currently existing achievable value of surface roughness, the high quality CZT wafers are of surface roughness values below about 1nm. Furthermore, studies on avoiding Angstrom-level extremely thin and shallow grooves are conducted to prevent possible surface oxidation formed on these morphological structures. These final polishing damages having depth of 0.1nm and width of 0.5nm have been observed by AFM techniques [25].

#### **4.10.2 Surface Oxidation**

For epi-ready CdZnTe substrates, it is important to prevent surface oxidation. Since the scratches or even Angstrom-level polishing damages might lead to localized oxidation [25], apparently, reducing the surface roughness is not sufficient to prevent oxidation. High quality CZT wafers are required to pack immediately after the inspection in an inert gas atmosphere. In addition, CZT wafers are subjected to bromine methanol (Br<sub>2</sub>-MeOH) solution having low bromine concentration (0.2%-0.5%) to remove oxide formed on the surface [9, 25].

#### **4.11 Total Thickness Variation**

As a physical property, the total thickness variation (TTV) throughout the CZT substrate surface is required to be as small as possible since any morphological variation such as warps leads to lower the quality of MCT epilayers. In order to avoid higher thickness variation values, CZT substrates are usually subjected to lapping process. It was reported that CZT wafers having dimensions 70 x 70 mm<sup>2</sup> have shown variation of 10µm or less in thickness. It was also reported that the thickness is less around the edge part of the wafers [9].

#### **4.12 Conclusions**

Chapter 4 presents the desired characteristics of CdZnTe substrates for MCT-based IR detectors in detail. Existence of impurities such as inclusions and precipitates is given. Besides, their effects on MCT epilayers and reduction of these impurities were also provided. Compositional Zn distribution throughout the substrate surface and how this non-homogeneity affects the lattice constant were explained. Another vital requirement, IR transmission related to the impurities was given. As a post growth processing, effects of annealing on the crystal quality and optical transmission were reported. Structural properties such as surface orientation, X-ray FWHM, and orientation accuracy were also provided. In addition, polarity concept in CZT

crystals, and measurement of average EPD were presented in brief. Electrical resistivity of CdZnTe substrates was stated. Finally, as physical properties, recent studies on reducing surface roughness, and surface oxidation were explained.

## CHAPTER V

# CHARACTERIZATION OF GROWN CADMIUM ZINC TELLURIDE CRYSTALS

### 5.1 Introduction

This chapter presents the results obtained from the CdZnTe growth studies. We have performed eight growth trials with different process conditions. Although some of the growth attempts were not successful, they all have been very useful to understand the process.

After each successful growth, CdZnTe ingots grown were subjected to wafer processing steps for characterization with the aim of obtaining a  $\text{Cd}_{0.96}\text{Zn}_{0.04}\text{Te}$  substrate having dimensions about  $5 \times 5 \text{ mm}^2$ , and relatively good technical specifications. These technical specifications aimed in this thesis study and the achievements at the end are given in different sections below. The details of both growth and wafer processing procedures in general, and those followed in this study were explained in Chapters 2 and 3, respectively. In the previous chapter, existing characterization techniques and results for commercial CZT substrates were described. In this chapter, characterization of CdZnTe substrates grown at METU is to be reported. As a general overview, throughout the thesis study, about eight (8) crystal growths were performed and five (5) of them produced ingots with sufficient crystal dimensions. Remaining three (3) growths yielded powder-structured (i.e. no bulk formation) CZT material. Among these five acceptable ingots, only two ingots

were found to have relatively high quality. Single crystalline CZT wafers with sufficiently large crystal sizes (i.e.  $\geq 5 \times 5 \text{ mm}^2$ ) could only be obtained from these two ingots named as ‘CZT-5’ and ‘CZT-7’.

## 5.2 Zinc Distribution Mapping of CdZnTe Wafers

The importance of Zn distribution homogeneity throughout the surface of CZT substrate was discussed in Section 4.3. Here, Zn distribution of CZT wafers grown at METU is given. SEM/EDS measurements have been performed to measure the Zn compositions of selected area on the substrate surface. Zn distribution was determined at about 10 different points on the surface to understand the variation. With the same EDS analysis, we were able to determine the composition of the crystal. Our aim was to obtain  $\text{Cd}_{1-x}\text{Zn}_x\text{Te}$  substrates where x value is close to 0.04 without applying any post growth annealing process.

Grown ingots were exposed to wafer processing steps including a series of slicing lapping and polishing processes as described in Chapter 3. After surface preparation of CZT wafers, SEM/EDS analyses were performed. Zn distribution of wafers obtained from the growths 4, 5, and 7 are given below. Besides, the same analysis was done for a commercial CdZnTe substrate with Chinese origin for comparison.

The results of the commercial sample having dimensions  $20 \times 20 \text{ mm}^2$  (figure 5.1) is shown in table 5.1.

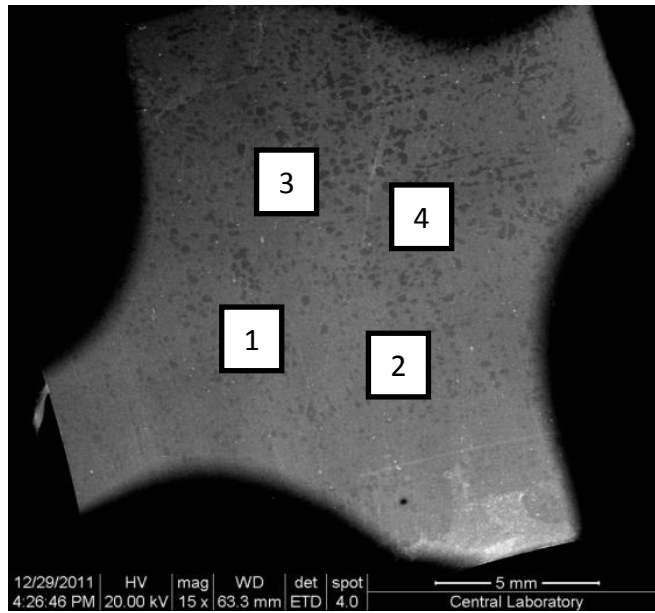


**Figure 5.1** Commercial CZT substrate with Chinese origin (20 x20 mm<sup>2</sup>)

As indicated in figure 5.1, four different areas were selected from the surface and the chemical composition was determined.

**Table 5.1** Zn distribution of the commercial CdZnTe substrate of Chinese origin

<b>Element</b>	<b>Region 1 @ 30keV (Atomic %)</b>	<b>Region 2 @ 30keV (Atomic %)</b>	<b>Region 3 @ 30keV (Atomic %)</b>	<b>Region 4 @ 30keV (Atomic %)</b>
<b>Cd</b>	48.43	47.45	48.22	48.54
<b>Zn</b>	2.81	3.52	3.71	2.84
<b>Te</b>	48.76	49.03	48.07	48.62
<b>x value</b>	5.48	6.91	7.14	5.53

According to table 5.1, we see that the commercial CZT substrate seemed to have relatively homogeneous Zn distribution since the EDS technique has an error percentage of at least 1%. Apparently, Zn concentration values given by the EDS measurement does not correspond to the x value of  $\text{Cd}_{1-x}\text{Zn}_x\text{Te}$  since these values are given for the total of 100% of CdZnTe. Therefore, one needs to subtract the Te amount and recalculate the x value by taking 100% as  $\text{Cd}_{1-x}\text{Zn}_x$ . x values calculated in this way are given in the last row of table 5.1. The variation seen in these values may have resulted from the uncertainty of the EDS technique. For this reason, we can conclude that the x values are within an acceptable interval around 0.04.

Similar analysis was performed for the samples we grew in our lab. The image of the sample we obtained from 4<sup>th</sup> growth (CZT-4\_1) is shown in figure 5.2. The surface of the sample was subjected to mechanical polishing and cleaning steps prior to the imaging.

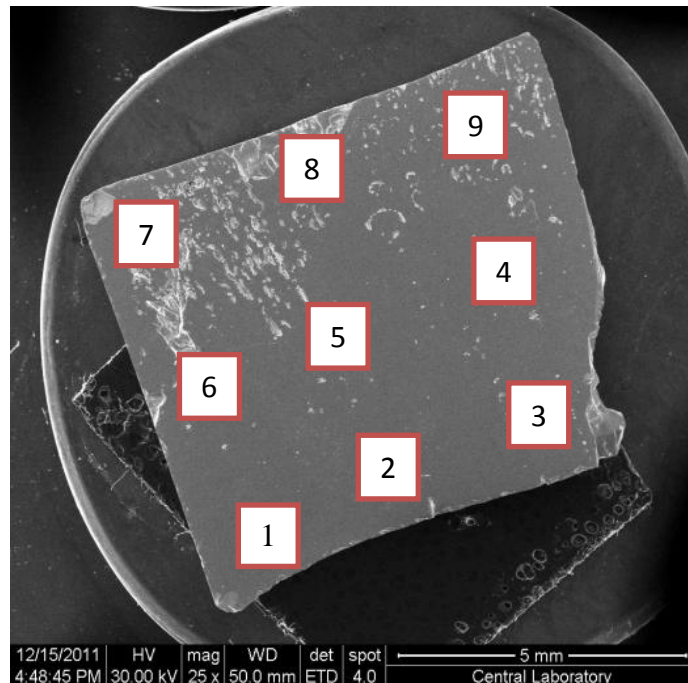


**Figure 5.2** Obtained slice (named CZT-4\_1) from the ingot CZT-4

CZT-4\_1 slice was the first successful growth after three efforts. Throughout this ingot, porous structure was observed, which is not acceptable for the preparation of epi-ready substrates. Nevertheless, Zn concentration distribution was studied as shown in Table 5.2.

**Table 5.2** Zn distribution of CZT-4\_1 slice grown at METU

<b>Element</b>	<b>R#1*</b>	<b>R#2*</b>	<b>R#3*</b>	<b>R#4*</b>	<b>R#5*</b>	<b>R#6*</b>	<b>R#7*</b>	<b>R#8*</b>	<b>R#9*</b>
<b>Cd</b>	48.55	48.11	48.81	48.89	48.31	48.36	48.58	47.75	48.24
<b>Zn</b>	2.57	2.58	2.25	2.59	2.68	2.74	2.70	2.66	3.44
<b>Te</b>	48.89	49.31	48.94	48.52	49.01	48.90	48.72	49.59	48.32
<b>x value</b>	5.03	5.09	4.41	5.03	5.26	5.36	5.27	5.28	6.66
* @30keV, atomic %, R: Region									

Despite its porous structure, Zn distribution of CZT-4\_1 sample was highly homogeneous. Zn percentage was a little higher than intended Zn percentage (i.e. 4%) though. Considering the uncertainty of the measurement system, we might expect even better actual values. Surprisingly, the homogeneity seems to be better than that measured from the commercial wafer (see table 5.1). For the CZT-4 ingot, we have studied the variation of Zn distribution in different regions of the ingot such as tail region, tip region, and middle region. In accordance with this purpose, slices were obtained from these regions and each slice experienced initial surface finishing procedures for EDS characterization. However, it was not possible to reach a conclusive generalization about the Zn distribution. In other words, two successive

slices obtained from any region (tip, tail, and middle) of the CZT-4 ingot have shown no systematic variation. This promising growth has led us to grow higher quality ingots such as CZT-5 and CZT-7 which are to be reported in the remaining part of this section.

CZT substrates were obtained from CZT-5 (figure 5.3) and CZT-7 (figure 5.4) ingots and Zn distribution analyses of them were performed.

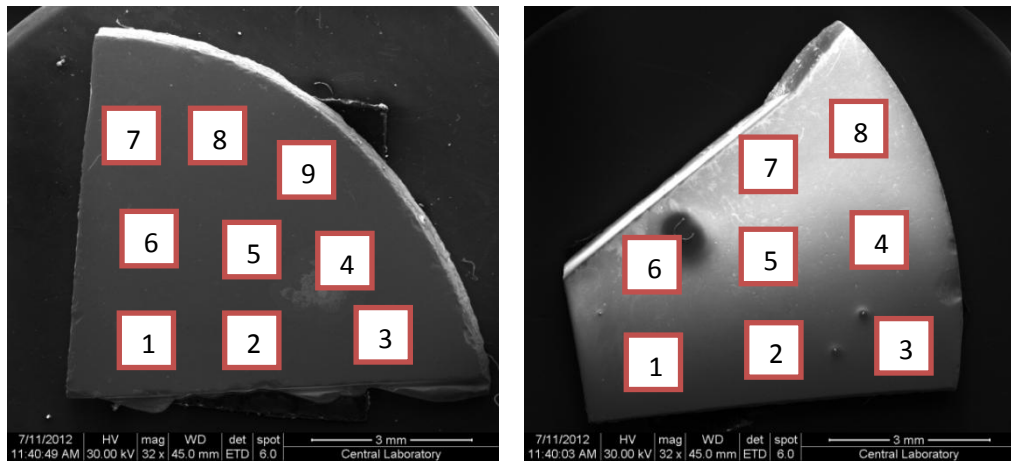


**Figure 5.3** (a) CZT-5\_1 slice, (b) CZT-7\_1 slice

Samples CZT-5\_1 and CZT-7\_1 experienced wafer processing steps described in Chapter 3. EBSD results have confirmed the single crystallinity of these samples. Zn distribution in these two CZT substrates seemed to be homogeneous and have consistent fashion with specified tolerances (Table 5.3) and (Table 5.4), respectively.

**Table 5.3** Zn distribution of CZT-5\_1 sample grown at METU

<b>Element</b>	<b>R#1*</b>	<b>R#2*</b>	<b>R#3*</b>	<b>R#4*</b>	<b>R#5*</b>	<b>R#6*</b>	<b>R#7*</b>	<b>R#8*</b>	<b>R#9*</b>
<b>Cd</b>	46.84	47.23	46.86	46.70	46.66	44.35	46.63	46.58	46.99
<b>Zn</b>	3.23	3.07	3.13	3.21	3.54	3.49	3.43	3.27	3.19
<b>Te</b>	49.93	49.70	50.02	50.10	49.80	49.82	49.94	50.15	49.82
<b>x value</b>	6.45	6.10	6.26	6.43	7.05	6.95	6.85	6.56	6.36
* @30keV, atomic %, R: Region									

Zn distribution of CZT-5\_1 sample is very homogeneous. However, with an average of 6.56%, x values are higher than the intended Zn (i.e. 4%) composition. The homogeneity observed in this growth is highly promising. The variation of Zn amount is only 1% in the CZT-5\_1 substrate.

**Table 5.4** Zn distribution of CZT-7\_1 sample grown at METU

<b>Element</b>	<b>R#1*</b>	<b>R#2*</b>	<b>R#3*</b>	<b>R#4*</b>	<b>R#5*</b>	<b>R#6*</b>	<b>R#7*</b>	<b>R#8*</b>
<b>Cd</b>	47.01	47.76	46.51	47.29	46.27	46.38	46.94	46.76
<b>Zn</b>	2.79	2.49	3.00	2.81	3.37	3.31	3.12	3.00
<b>Te</b>	50.20	49.75	50.48	49.90	50.35	50.31	49.94	50.23
<b>x value</b>	5.60	4.96	6.06	5.61	6.79	6.66	6.23	6.03
* @30keV, atomic %, R: Region								

Similar to previous samples stated above, CZT-7\_1 has a homogeneous Zn distribution throughout the wafer surface. Zn mole fraction was found to be 5.99% on average, which is also above the intended value (4%), but less than the previous growth.

This time, variation in the Zn percentages obtained is nearly 2% which is slightly higher than the previous growth.

Figure 5.4 shows the variation of Zn distribution across the surface of the two samples (CZT-5\_1 and CZT-7\_1). We see that Zn distribution have the same tendency in both samples and the variation is within acceptable range.

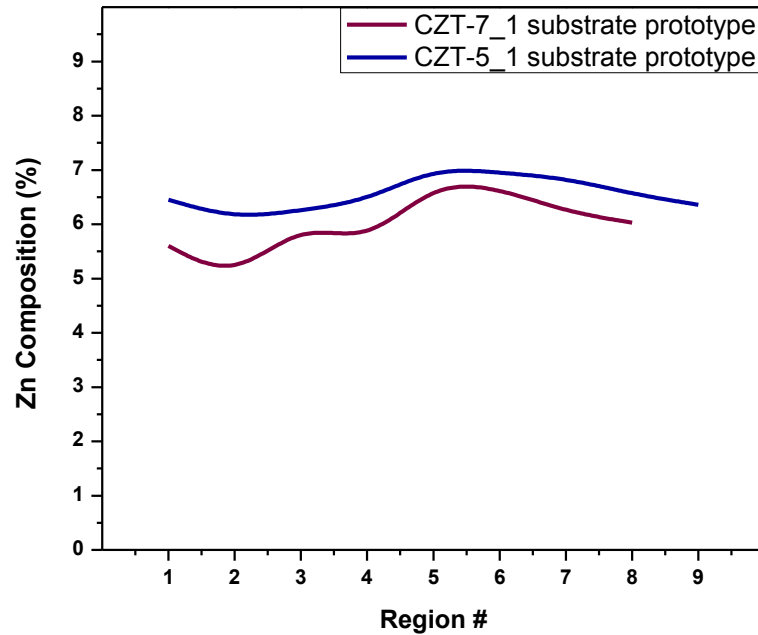


**Figure 5.4** Zn distribution tendency of samples CZT-5\_1 and CZT-7\_1

### 5.3 Infrared Transmission

In a CdZnTe crystal, Te precipitates are known to be the primary factor degrading the infrared transmission as explained in Section 4.4. Generally, in the wavelength interval 2-20  $\mu\text{m}$ , 60% and more IR transmission (IRT) values of about 800 $\mu\text{m}$ -thick CZT substrates are acceptable for MCT based devices fabricated on it.

IR transmission measurements of CdZnTe slices were performed using Bruker Equinox 55 FTIR Spectrometer within the wavelength interval 2-20  $\mu\text{m}$ . At the beginning of this work, we aimed to obtain 800 $\mu\text{m}$  thick CZT substrate with IR transmission values higher than 30% in the wavelength interval of 2-20  $\mu\text{m}$ .

For the slice CZT-4\_1, obtained from the ingot CZT-4, IR transmission was below 15% as shown in figure 5.5. This IRT result was far from the intended transmission behavior.

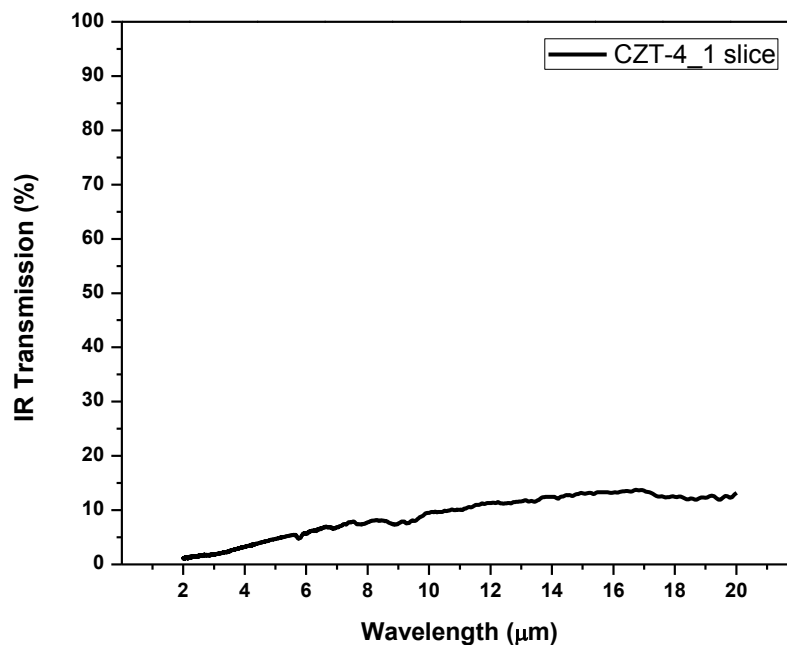
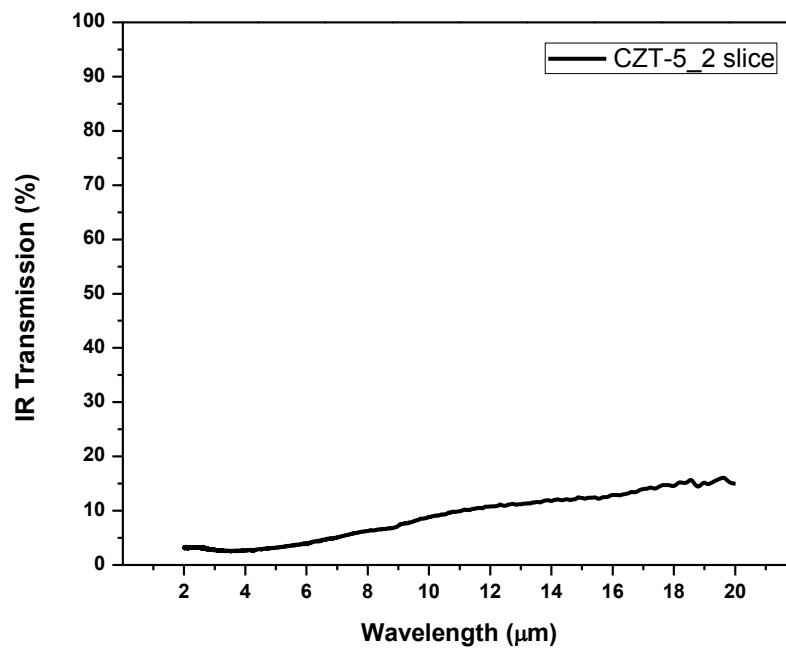


Figure 5.5 IR transmission of 850 $\mu\text{m}$ -thick CZT-4\_1 slice

Since this ingot was of porous structure, it was not possible to obtain slices having better surface quality (i.e. porous free). The low IR transmission behavior of CZT slice was apparently due to having more than one grain, the low quality crystal structure, dislocations, and impurities.

Similarly, single side polished slices from the ingot CZT-5 were characterized for IR transmission. As shown in figure 5.6, the IR transmission of the sample CZT-5\_2 is not better than the samples obtained from CZT-4.



**Figure 5.6** IR transmission of 850μm-thick CZT-5\_2 sample

Although this ingot (CZT-5) appeared to be more uniform and having a porous-free structure, its IRT behavior is similar to what we observed for CZT-4 samples. The low IRT might have resulted from the low crystal quality indicated by the multi-grain structure and the micro-defects present in the crystal. We also know that single side polishing is not sufficient for a good IR transmission. It is however, surprising to see that gross differences we observed between these samples do not generate different IRT behavior. Indeed, from the EBSD results, we observed that this slice from the CZT-5 ingot was not having a single crystal structure. We later obtained single crystal regions from the same ingot and wafers cut from this part of the ingot showed excellent IR transmission behavior as presented below.

Figure 5.7 shows the IRT data for a double-side polished slice obtained from CZT-7 ingot. We obtained IR transmission higher than 30% in the 2-20  $\mu\text{m}$  wavelength interval. However, as we see from figure 5.7 that the transmission value depends on the wavelength within the measurement interval. This variation is not desirable for MCT-based IR technology. We know from other measurements that the crystal quality of this sample was improved with respect to the previous samples. Clearly, the transmission is very much correlated with the quality of the crystal.

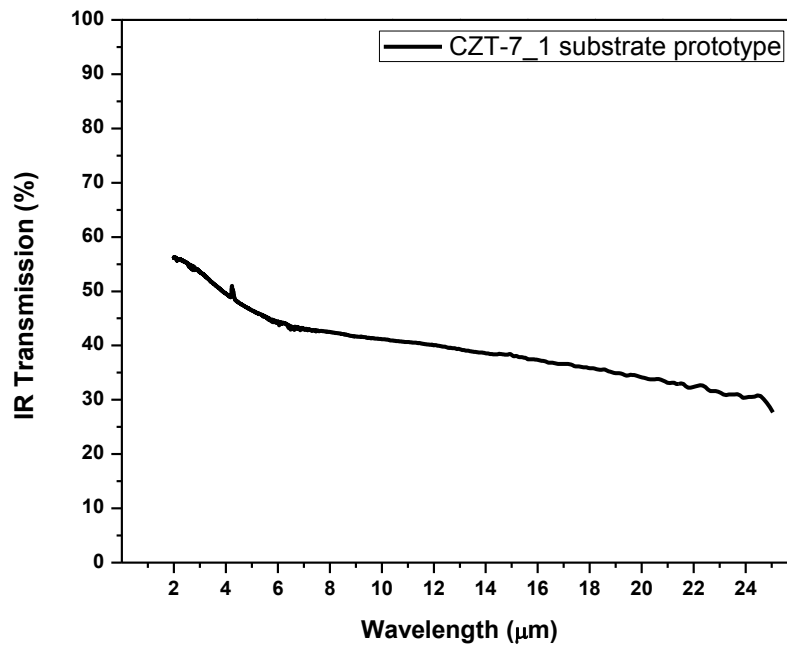


**Figure 5.7** IR transmission of 830μm-thick CZT-7\_1 sample

The observed IR transmission behavior showed similarities with the previously published work [39] in which they also showed the carrier concentration dependence, additionally.

For comparison, we measured the IRT values of the commercial CZT sample with Chinese origin. This showed a flat infrared transmission value near 60% (around 55%, indeed) as shown in figure 5.8.

In order to achieve such encouraging transmission value near 60%, a new slice with single crystal structure was singled out from the CZT-5 ingot. This sample was subjected to double-side polishing using fine polishing steps and was thinned down to around 820μm. CZT-5\_1 was totally single crystal. As shown in figure 5.9, this sample shows much superior IRT behavior.

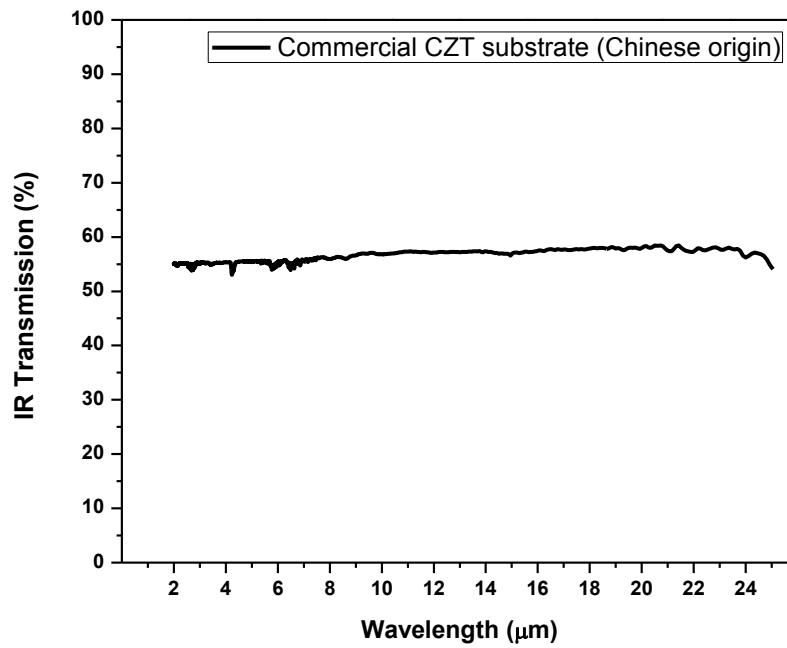


Figure 5.8 IR transmission of 820μm-thick commercial CZT wafer with Chinese origin

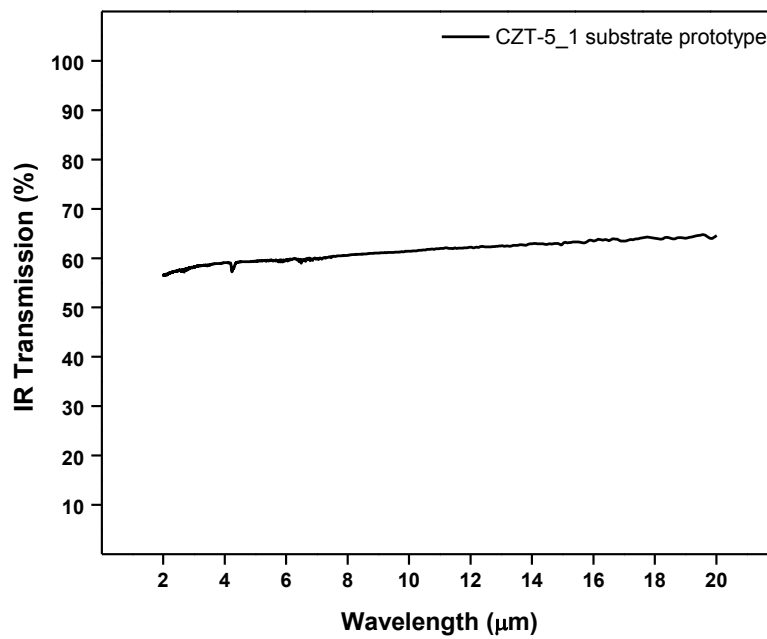


Figure 5.9 IR transmission of 820μm-thick CZT-5\_1 sample

CZT-5\_1 sample was reported to have the highest IR transmission value obtained in the CZT studies we carried out. On average, approximately 59% IR transmission value was achieved within the interval 2-20  $\mu\text{m}$  for this sample. This result is at least as good as that obtained from the commercial CZT substrate. This promising result indicates that we have reached a good crystal quality with less density of Te precipitates, impurities, and crystalline imperfections.

#### **5.4 Polarity Determination of Grown CdZnTe Wafers**

Since the crystal polarity of CZT wafers is crucially important for epitaxial MCT growths, it is necessary to determine the polarity of the surface. As we described in Section 4.7, the polarity can be determined by a practical technique based on chemical etching with a mixture of three acids in the form of HF:HNO<sub>3</sub>:lactic acid (1:1:1 v), which we call Brown solution. The single crystal sample, CZT-5\_1, was dipped into the prepared Brown etchant solution for not longer than a minute; then rinsed with deionized water, immediately. Following the etching process, surprisingly good color difference was observed between two sides of the sample. The surfaces were labeled as 'A' and 'B' for matt black and bright shiny surfaces, respectively. Although this etchant was reported to be most efficient for {111} faces, we have observed that this polarity determination method provided fast, reliable, and efficient results for other faces as well.

#### **5.5 Etch-Pit Density Measurements of CdZnTe Wafers**

To determine the etch-pit density (EPD), CZT slices were subjected to various etchants and methods such as Everson and Nakagawa as described in Section 4.8. Next, the resultant surfaces were inspected to observe the pit formation using scanning electron microscope.

Since the effectiveness and reliability of the EPD determining etchants are still controversial, in order to obtain desired pit patterns on the surfaces, we performed a

series of different etching trials on slices selected from various growths. Prior to EPD determination studies, first the etching method was determined.

Initially, Nakagawa method was used [34]. CZT-6\_1 slice from the ingot CZT-6 was selected for this etching trial. CZT-6\_1 slice was of porous free structure and good quality surface; however, it contained at least more than ten grains including the (111) crystal orientation. Next, the etchant solutions,  $\text{H}_2\text{O}:\text{HNO}_3:\text{K}_2\text{Cr}_2\text{O}_7$  ( $10\text{cm}^3:5\text{cm}^3:2\text{g}$ ) and  $\text{H}_2\text{O}:\text{H}_2\text{O}_2:\text{HF}$  ( $20\text{cm}^3:20\text{cm}^3:30\text{cm}^3$ ), were prepared. From now on, the former etchant solution is named as E-reagent. CZT-6\_1 slice was first subjected to E-reagent for a minute, then the  $\text{H}_2\text{O}:\text{H}_2\text{O}_2:\text{HF}$  solution was applied for 20 seconds. Finally, the slice was then dipped into E-reagent for less than 1 second to remove oxide layer on the surface. The resultant surface of the CZT-6\_1 slice is shown in figure 5.10.

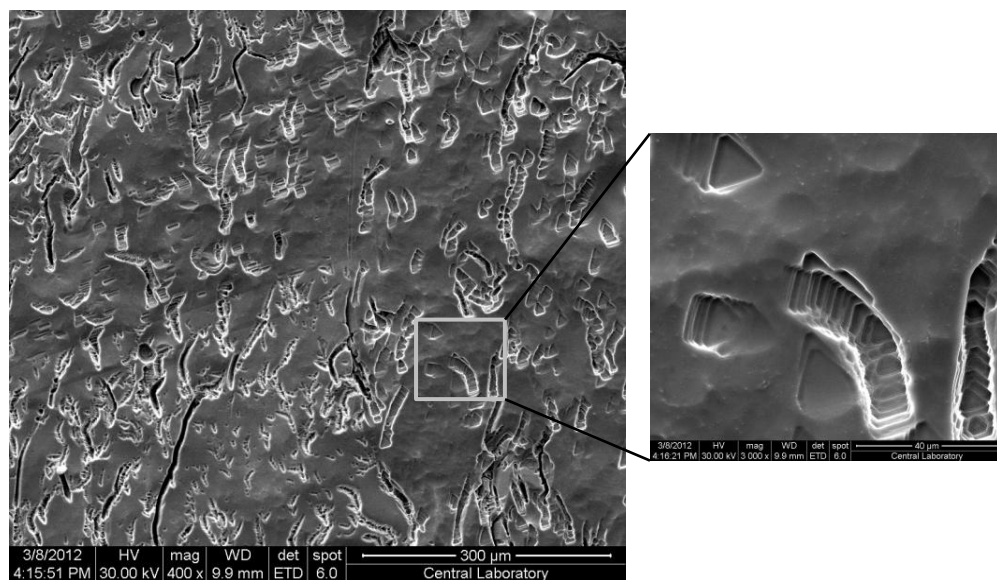


**Figure 5.10** Etch-pit formation on CZT-6\_1 slice

From the images, we see the formation of triangular-shaped etch-pit formation on this sample. Similar pit formations were observed by Bissoli et al. in 2005 [40], and were attributed to the dislocations. In our case, triangular pits are not well separated; therefore, not easily countable. We observe that the number of pits is enhanced by the multi-grain structure in the sample.

In addition to the triangular-shaped pit formation on CZT-6\_1, round-like shaped or somewhat hexagonal pits were also observed near the triangular pits as seen from figure 5.11.

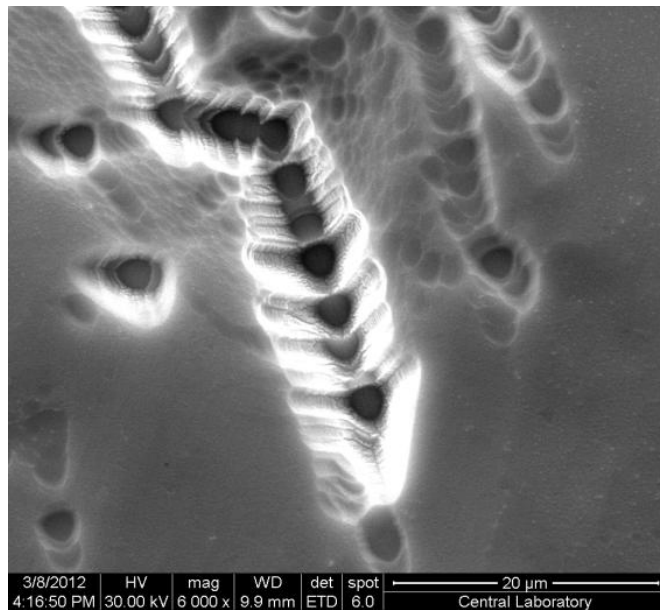


**Figure 5.11** Hexagonal or round-like pits formed on CZT-6\_1 slice

It is known that these round-like shaped pits provide information about distribution of Tellurium inclusions. Formation of these pits showing Te inclusions was revealed by the E-reagent exposure, which is commonly used in both Nakagawa and Inoue etching methods. Besides, E-reagent is not a selective etchant and indeed, it is used as a chemical etchant for damage removal and activation of the surfaces [40].

Due to multi-grained structure of the slice CZT-6\_1 and overlapped etch-pit pattern, calculation of average EPD could not be performed.

As an alternative etchant, Everson etch which has the composition of HF:HNO<sub>3</sub>:Lactic acid (1:4:25 v) was applied to the slice CZT-5\_3 for about 2.5 minutes. After etching, the etch pattern shown in figure 5.12 was obtained. We see that we obtained a remarkable structure which does not resemble the expected surface pit formation.

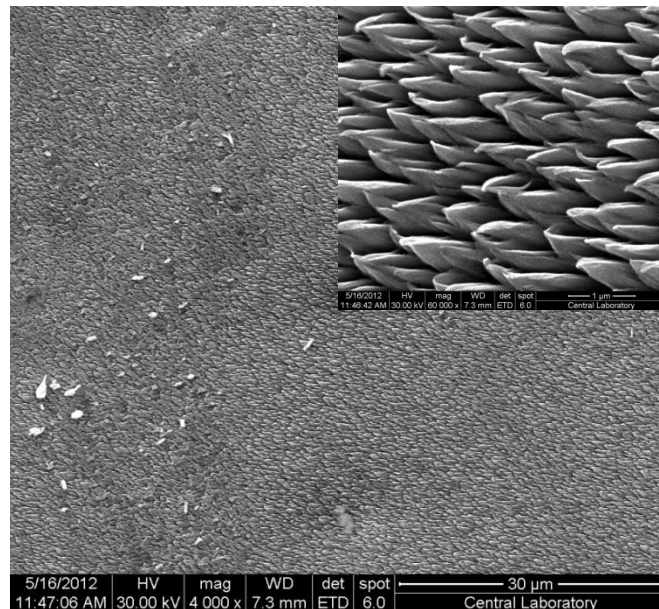


**Figure 5.12** Etch pattern formed on CZT-5\_3 after Everson etching

Another etch trial that we tried is based on Bromine-methanol solution. This etchant was applied to the sample CZT-5\_4, immediately after the Everson etch. Etch pattern was similar to the Everson etched CZT-5\_3 sample (Figure 5.13).

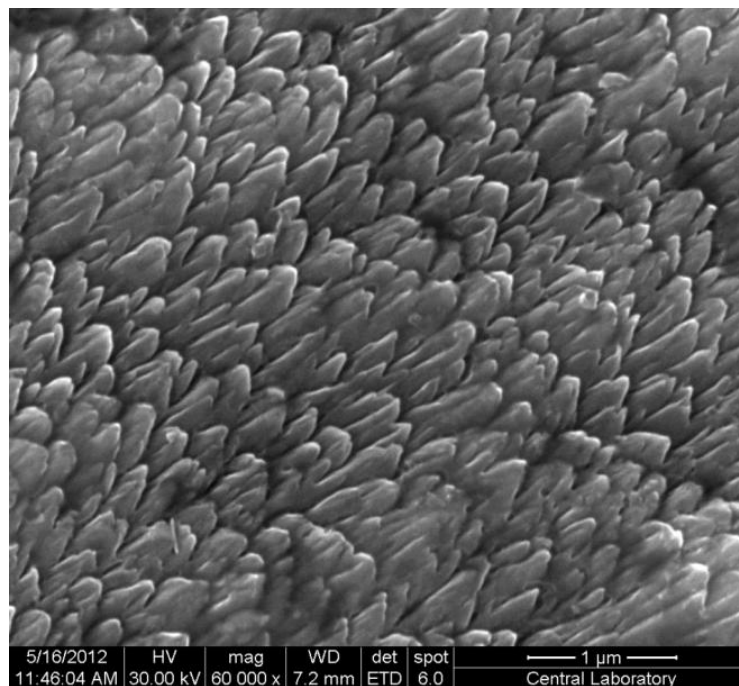


**Figure 5.13** Etch pattern formed on CZT-5\_4 after Everson etching + Br<sub>2</sub>-MeOH

With these etching trials, we did not obtain an appropriate etch pit formation to calculate the average EPD. Each etching method produced different morphological structure on the surfaces of slices.

Finally, we applied the Nakagawa etching to a single crystal slice from CZT-5 for a minute. The result shown in figure 5.14 is more promising. Although the pattern is

different than commonly observed ones, it allows us to determine the density of etch pit. We conclude that a multi grain surface does not provide the required etch pattern to obtain EPD.

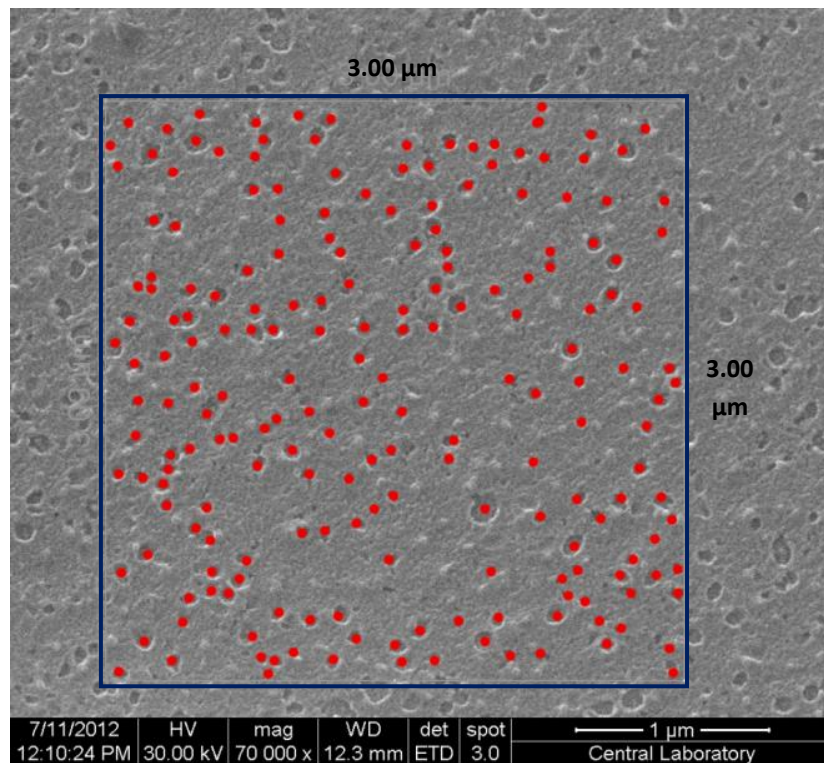


**Figure 5.14** Etch pattern formed on CZT-5\_5 after E-reagent exposure

Round-like shaped pits were counted on a specified area of  $3 \times 3 \mu\text{m}^2$  of this sample. From this count, the total average EPD was calculated as  $2 \times 10^9 \text{ cm}^{-2}$ . Although this value represent a relatively good achievement for this study, it is still higher than the required density values. It should be also noted that the pits formed on the surface are nanoscale.

## 5.6 Resistivity Measurements of Grown CdZnTe Wafers

As stated in Section 4.9, CZT substrates having resistivity around  $10^3 \Omega\text{cm}$  are used for MCT epitaxy. Our goal was to obtain CZT wafers having resistivity values higher than  $10^3 \Omega\text{cm}$ . Resistivity of CdZnTe slices grown in our lab was measured by the electrical measurements (i.e. I-V characteristics).

For the electrical connection, Cu-Au electrodes with contact area of  $1\text{mm}^2$  and length of 5mm was thermally evaporated on the surface of the CZT-5\_6 slice. Cu-Au was used to obtain an Ohmic contact. Ohmicity of contacts were also checked. The I-V characteristics of this CZT slice was measured at 77K. As shown from the result displayed in figure 5.15, an almost Ohmic behavior was obtained. Using the slope of this I-V curve, the resistivity value at 77K was calculated as  $1.5 \times 10^7 \Omega\text{cm}$ . This value is quite satisfying the requirement for the subsequent epitaxial growth.

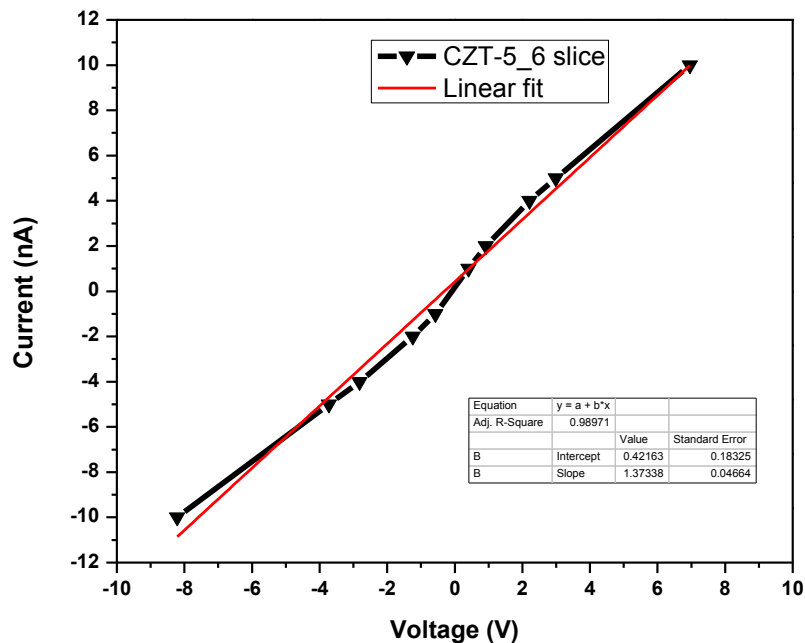


Figure 5.15 Current-Voltage characteristics of CZT-5\_6 at 77K

## **5.7 Crystallographic Surface Orientation Measurements**

In this study, our primary aim was to obtain a single crystalline CZT wafer with at least 5 x 5 mm<sup>2</sup> area. We tried to obtain the highest crystal yield from grown ingots having diameters up to 17mm independent from the orientation constraint; yet the CZT prototypes having (211) surface orientation would fulfill our ultimate requirement. Alongside with this purpose, ingots were sliced as instructed in Chapter 3. Slices either perpendicular or parallel to the growth direction were obtained. Cutting in reference to a specific angle was not possible due to restricted capability of the slicing systems. Surface orientation measurements were performed by XRD (X-ray diffraction) and EBSD (Electron backscatter diffraction) measurements.

### **5.7.1 Surface Orientation Measurements by XRD**

Slices having multi-grain structure were initially characterized by X-ray diffractometer to observe the most preferred crystal plane peaks. In this case, we expect to obtain multi-peak pattern corresponding to the crystal planes of the grains. If a single domain with sufficient crystal quality can be singled out from the rest of the sample, one should expect a single XRD peak in the spectrum. This was accomplished by dicing of CZT wafers to single out the marked area.

Initially, CZT-7 ingot was sliced to obtain a wafer with ingot diameter. XRD spectrum of this sample is seen in figure 5.16.

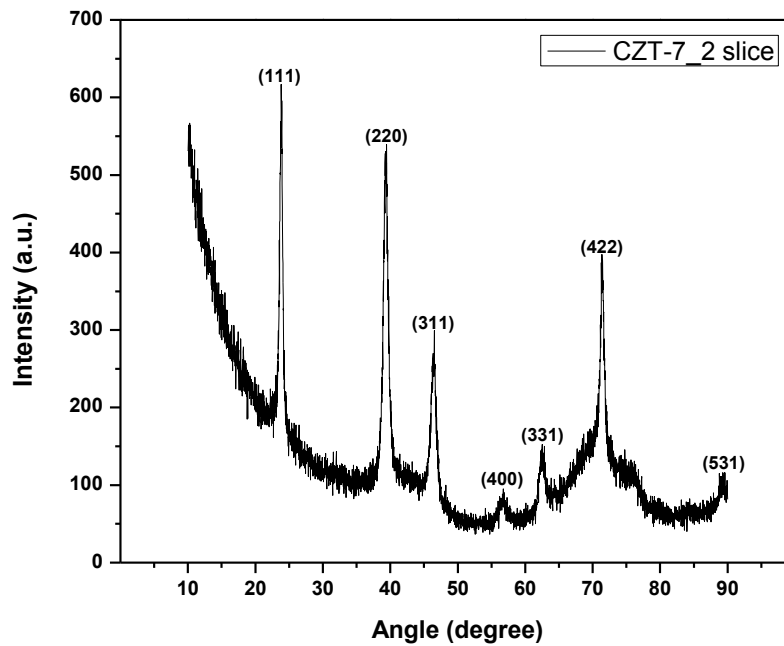


**Figure 5.16** X-ray diffraction spectrum of CZT-7\_2 slice

As expected, this XRD spectrum shows the XRD signals corresponding to the planes parallel to the sample surface. It was seen that x-ray signals belonging to (111) and (220) faces are sharper and stronger than the (422) - i.e. (211) - signal. Here, the existence of (422) peak is of great importance for the CZT studies, and in remaining part of the study, (211) orientation was traced. Next, this CZT-7\_2 slice was diced along the grain boundaries to obtain the single crystalline regions. Region having surface orientation of (211) was named as CZT-7\_1 and this slice was processed as a main sample of this study. CZT-7\_1 wafer was then characterized by X-ray diffractometer as shown in figure 5.17.

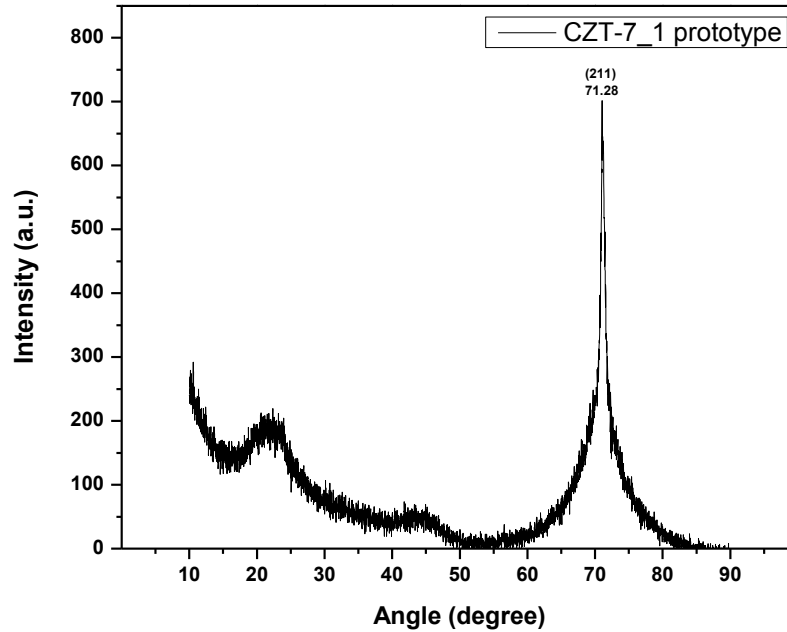


**Figure 5.17** X-ray diffraction spectrum of CZT-7\_1 prototype

CZT-7\_1 slice was singled out from the CZT-7\_2 slice with ingot diameter. By visual inspection, the CZT-7\_1 slice was expected to have single crystalline structure. The XRD spectrum obtained from this single crystal piece is shown in figure 5.17. We see that the XRD peak corresponding to (211) plane dominates the spectrum. This is providing that this diced piece has almost single crystal structure with the (211) surface orientation. It is remarkable that we obtained (211) orientation without any particular procedure. In addition to the major (211) peak, we see minor XRD signals (i.e. peaks) corresponding to the planes (111) and (311) at the diffraction angles  $23.75^\circ$  and  $46.47^\circ$ , respectively. However, from the FWHM of the peak of (422) plane, it can be deduced that the crystal quality of CZT-7\_1 is not at the desired level. A detailed crystal quality analysis will be given in Section 5.8.

## 5.7.2 Surface Orientation Measurements by EBSD

EBSD is a powerful measurement system in which the electron beam is used to determine crystallographic orientation at micrometer scale. For a micro-diffraction experiment, the probe size must be smaller than the size of the microstructural units. For this reason, electron beam is an ideal tool for the micro diffraction experiment. EBSD determines the crystal domain very accurately.

Throughout the EBSD studies conducted in our lab, our aim was to identify the regions with the single crystal structure. For this purpose, various CZT slices were prepared and tested. Most of slices studied had at least two different surface orientations. The most promising result was observed in the analysis of CZT-7\_1, shown in figure 5.18.

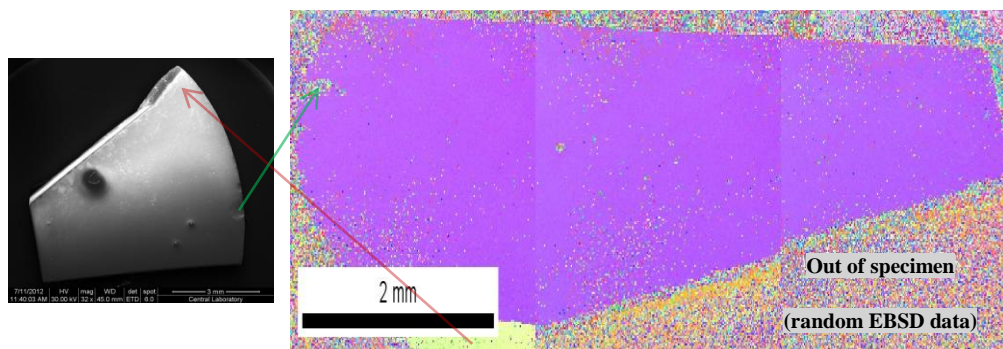


**Figure 5.18** EBSD map of CZT-7\_1 slice shown in the SEM picture (on the left). Different orientations are color coded.

Purple region in the EBSD analysis shows that we have obtained large crystal domain with single crystal structure in the CZT-7\_1 slice. Small amount of noisy data points can be avoided by preparing better substrate surfaces and reducing the

analysis' step size. Step size is the length between the micro-diffraction points. EBSD excellence offers down to 1 $\mu$ m step size. During the EBSD analysis we carried out, the system automatically divided the substrate surface into three parts (figure 5.19) and each part was analyzed successively.

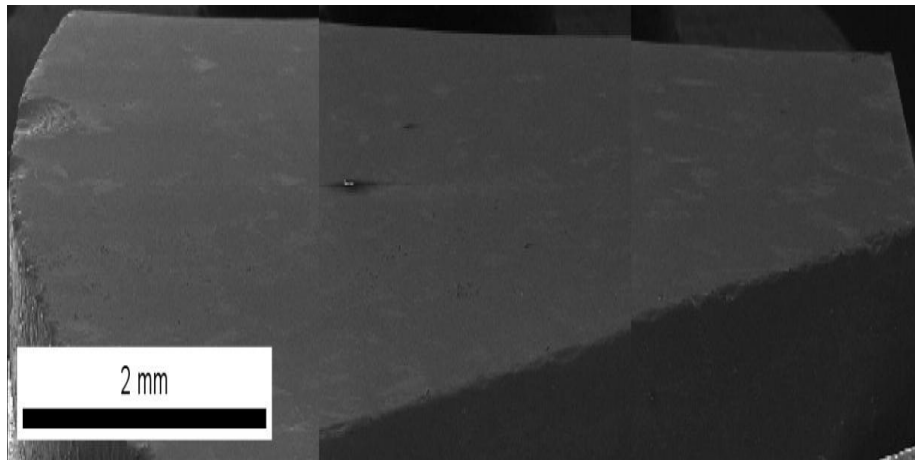


**Figure 5.19** SEM image of CZT-7\_1 prototype

For orientation determination, EBSD offers another map called “inverse pole figure map” as shown in figure 5.20. Each point or pixel on the map corresponds to a specific orientation indexed with Miller indices  $hkl$ .

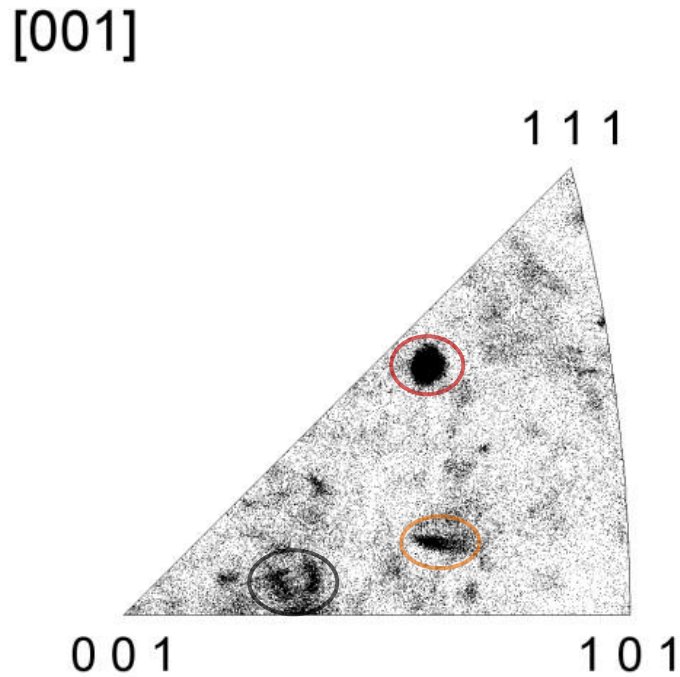


**Figure 5.20** Inverse pole figure (IPF) map of CZT-7\_1

Results of the EBSD analysis of CZT-7\_1 have shown that black spot encircled in red corresponded to the (211) crystal orientation and exact ( $hkl$ ) value was 8, 9, and 17 respectively. Other two spots encircled in orange and black may explain the existence of small grains and even subgrains in the CZT-7\_1 sample, and the noisy data. Both XRD and EBSD results have shown consistent results.

## 5.8 X-ray Rocking Curve Measurement

As discussed in Section 4.6, the quality of crystals can be determined by performing X-ray rocking curve measurements. Smaller peak widths (i.e. smaller FWHM values) are the signs of better crystal quality.

X-ray rocking curve measurements of crystals require high resolution X-ray diffraction (HRXRD). In rocking curve (RC) measurements, Germanium monochromator is used for higher resolution.

Since the crystal quality of CZT-7\_1 prototype was low, we could barely obtain a rocking curve signal. This was experienced because Germanium monochromator degrades the total intensity of the signal in order to perform high resolution RC measurements. From the sample CZT-7\_1 we have obtained a FWHM value of 922 arcsec. This value indicates that the crystal quality is not at desired level. Initially, the CZT sample having (211) orientation and below 1000 arcsec FWHM value is much higher than the commercially available wafers.

## **5.9 Crystallographic Misorientation Analysis**

Since the rocking curve measurements could not be performed properly for the whole crystal, crystallographic orientation could not be determined from the RC analysis. For this reason, EBSD analysis was used to determine the misorientation. Using EBSD statistical data analysis software, deviation from the (211) surface orientation was determined statistically as shown in figure 5.21. It is found that about 41% of the microdiffraction points analyzed had a misorientation angle of  $2.35^\circ$ . Remaining 59% of the points displayed the contribution of deviation points having percentages below 1%. As it can be seen from this analysis, crystal structure is of low quality although the dominant misorientation is  $2.35^\circ$ . Behavior of the remaining 59% of the analyzed points may be due to the existence of small grains and even subgrain formation in the crystal. However, notice also that any noisy data point leads to bad analysis results. This is because noisy data point will act as if it was randomly misoriented; so that contribution to misorientation from the reference orientation increases.

In order to understand the dramatic effect of noisy data points, relatively smaller regions were selected for similar analysis as shown in figure 5.22. In this case, we see only one misorientation value which is dominant in the statistical distribution.

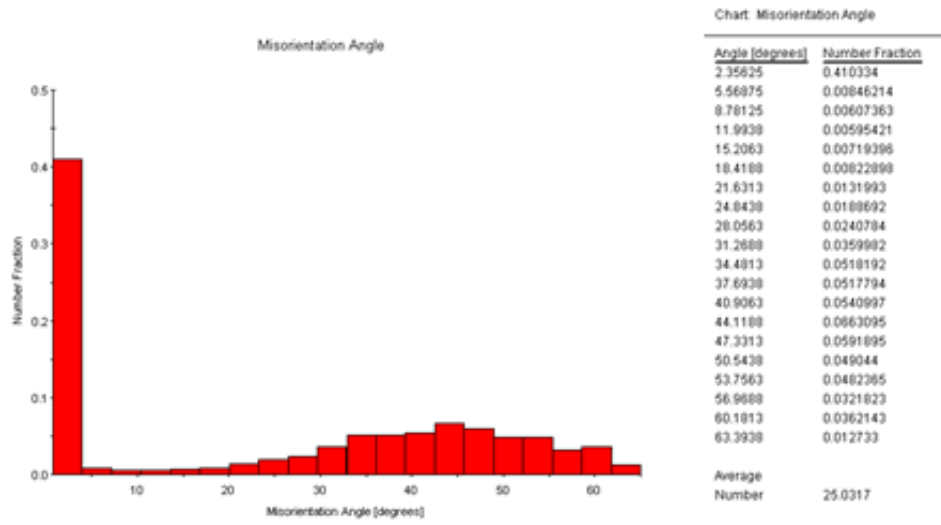


**Figure 5.21** Misorientation angle distribution of CZT-7\_1 prototype in reference to (211) plane

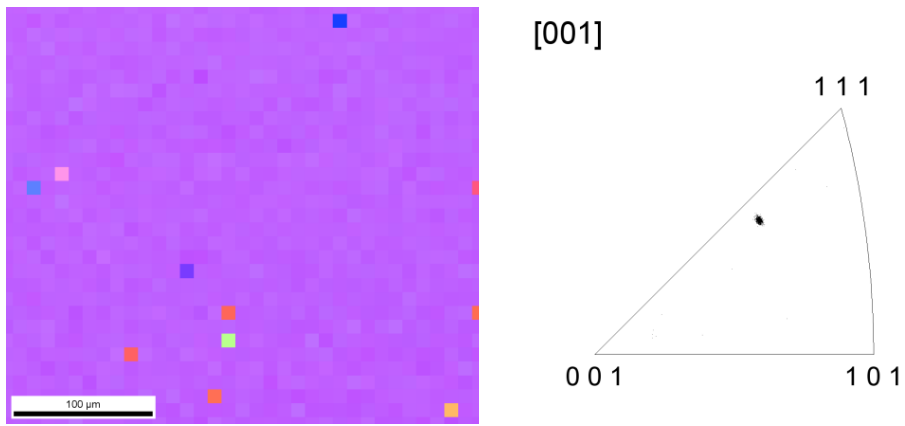


**Figure 5.22** 100µm-scaled noise free and single crystalline selected area

In figure 5.22, single crystalline area having a scale of 100 $\mu$ m was selected for analysis. The IPF map shows the noise free data. Misorientation analysis was performed for this specified region (figure 5.23).

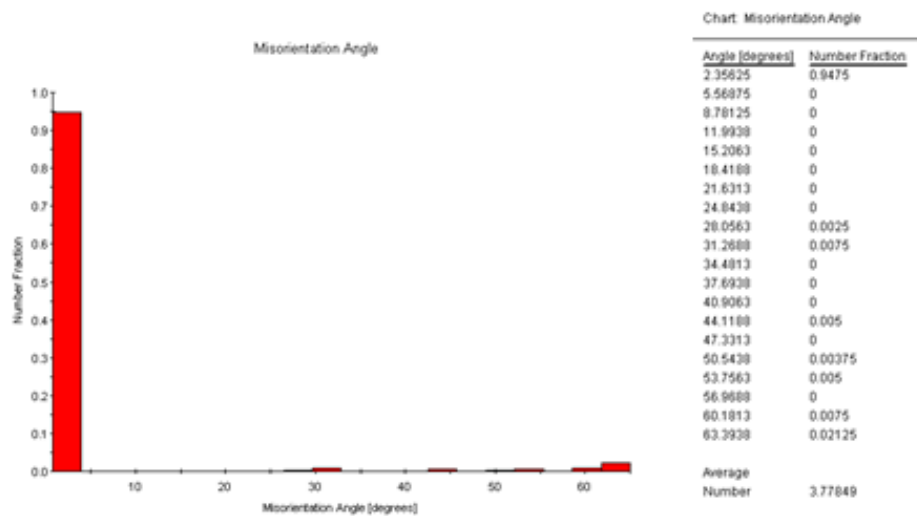


**Figure 5.23** Misorientation angle distribution of CZT-7\_1 prototype

Noisy data point effect was clearly observed after the EBSD data analysis above. About 94% of the data points were of misorientation angle of 2.35°. So, it can be concluded that this CZT-7\_1 sample has a (211) crystal orientation with a misorientation angle of 2.35°. Nevertheless, this conclusion is supported well when the percentage value (94%) becomes 100%. This can be accomplished by preparing noise free prototype surfaces. Figure 5.24 has shown the importance of having high quality surfaces. Here, 40 $\mu$ m-scaled region was selected and the percentage of points having misorientation of 2.35° was observed to be 100%.

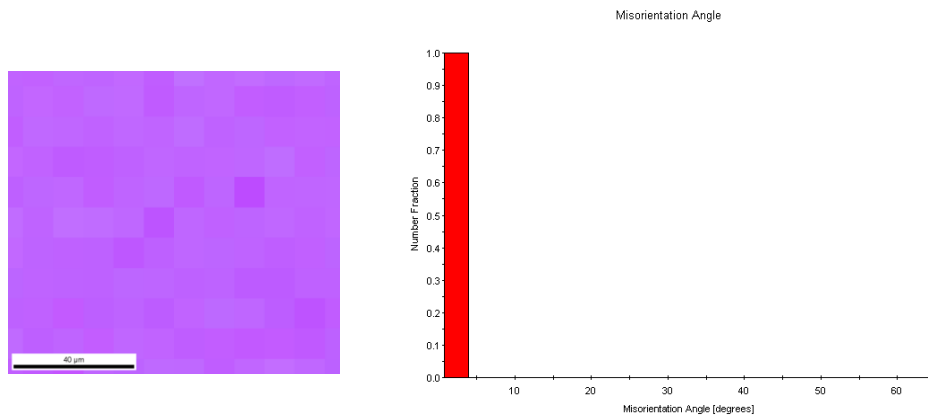


**Figure 5.24** 40μm-scaled selected area and misorientation angle distribution of CZT-7\_1 sample in reference to (211) crystal orientation

## 5.10 Conclusions

Throughout the Chapter 5, we have presented results of characterization studies of grown CdZnTe crystals. Most of the characterization techniques described in Chapter 4 were applied. As CZT characteristics, Zn distribution throughout the wafer surface, and crystal polarity determination were investigated. Measurements including etch-pit density, IR transmission, resistivity, and surface orientation measurements were also performed and their corresponding results were discussed in detail. Crystal qualities of grown CZT substrates were determined by X-ray rocking curve measurements. EBSD studies played a key role in determining the surface orientation and the orientation accuracy. Zn distribution was observed to be homogeneous, and the process of polarity determination of a CZT wafer was optimized. Various EPD trials provided crucial information about dislocations and Te precipitates. Obtained IR transmission was very promising for future studies.

## CHAPTER VI

### CONCLUSION AND FUTURE STUDIES

This thesis reports on the growth and characterization of  $\text{Cd}_{0.96}\text{Zn}_{0.04}\text{Te}$  crystals grown in three-zone vertical Bridgman furnace. Growth process of CdZnTe is challenging due to thermo-physical properties which leads to twin formation and uncontrolled lattice defects during the cool-down step of the growth. In this thesis work, bulk-growth of CdZnTe was realized and several characterization techniques were employed. Large area (at least 5mm x 5mm) single crystalline CdZnTe slices with (211) crystal orientation were produced and characterized.

Electron backscatter diffraction (EBSD), Fourier Transform Infrared Spectroscopy (FTIR), X-ray Diffraction (XRD), and Scanning Electron Microscopy (SEM) with Energy Dispersive Spectroscopy (EDS) techniques were intensively used to study various aspects of the grown CdZnTe material.

Following the growth of bulk material, thin slices were obtained by cutting using either diamond blade annular saw or wire saw system. Almost all of the inspected slices were subjected to lapping, mechanical polishing, and chemical etching prior to the characterization. We obtained very good Zn homogeneity throughout the CZT slices; however, in some cases the mole fraction of Zn was found to be slightly higher than the intended Zn composition (i.e. 4%). Single crystallinity of the CdZnTe slices was confirmed by EBSD measurements. Moreover, crystallographic misorientation from the (211) orientation was found to be  $2.35^\circ$  by EBSD analysis.

Infrared transmission of 60% was achieved, which is showing the reduced density of Tellurium inclusions/precipitates. Nevertheless, the XRD results indicate low crystal quality. This is probably due to the presence of subgrains and defects in the bulk of the grown crystals. The etch pit density experiments were carried out to reveal the defect density in the grown crystal. We measured the average etch pit density as  $2 \times 10^9 \text{ cm}^{-2}$  in our samples. In agreement with the XRD rocking curve analysis, this density is higher than the generally accepted value ( $10^4$ - $10^6 \text{ cm}^{-2}$ ). In spite of the results we obtained from the EPD and XRD analysis, we were not able to reveal the defect structure and the density unambiguously.

As an electrical characterization, resistivity of the grown CdZnTe crystal was measured at 77 K and calculated as  $1.5 \times 10^7 \text{ } \Omega\text{cm}$ . The resistivity of the CZT crystal is desired to be as high as possible to prevent any electrical interference from the substrate during the MCT photodiode operation. The measured value was compared with the resistivity values and found to be satisfactorily high. This might be surprising when considering the XRD and EPD experiments; however, we believe that the low resistivity is related to the Te inclusion which is successfully eliminated in our growths.

Characterization results have shown that we have successfully grown CdZnTe ingots using an old-fashioned Bridgman furnace having instabilities in temperature control during the crystal growth. Many of the crystal properties such as IR transmission, single crystallinity, surface orientation (211), electrical resistivity, are all satisfying for a subsequent MCT growth. It is clear that the crystal quality needs to be improved with more detailed and focused studies which might require a more developed furnace system.

With this background and perspective, we aim to continue our work to improve the crystal quality of CdZnTe substrates by further optimizing the growth parameters, such as pull rate and temperature gradient. The crucible material and shape effects on crystal quality can be investigated using a stable growth furnace. As a new approach, precompounding effect can be observed after performing a series of CdZnTe growths. We can also study the effect of post growth processes (annealing) that can improve the crystal quality.

As a future work, high quality CdZnTe substrates can be obtained using high quality growth systems following to these promising results obtained from this CdZnTe study.

Specifically, as a growth detail, crucible material and shape effects on crystal quality can be investigated using stable growth furnace. Besides, precompounding effect can be observed after performing a series of CdZnTe growths. Finally, high quality larger diameter ingots can be grown using well controlled multi-zone growth furnace.

## REFERENCES

- [1] W. Lawson, S. Nielsen, E. Putley and A. Young, "Preparation and Properties of HgTe and Mixed Crystals of HgTe-CdTe," *Journal of Physics and Chemistry of Solids*, pp. 325-329, March 1959.
- [2] P. Norton, "HgCdTe Infrared Detectors," *Opto-Electronics Review*, pp. 159-174, 2002.
- [3] A. Rogalski, "Recent Technologies in Infrared Detector Technologies," *Infrared Physics & Technology*, pp. 136-254, 2011.
- [4] G. Gaussorgues, *Infrared Thermography*, London: Chapman & Hall, 1994.
- [5] O. O. Cellek, "Ensemble Monte carlo Simulation of QWIPs, and InP Based Longwavelength QWIPs for Thermal Imaging," Ph.D Dissertation, Middle East Technical University, Ankara, 2006.
- [6] E. A. Plis, "Mid-IR Type-II InAs/GaSb Nanoscale Superlattice Sensors," Ph.D Dissertation, The University of New Mexico, Albuquerque, New Mexico, 2007.
- [7] P. Capper, *Properties of Narrow Gap Cadmium Based Compunds*, London: INSPEC, 1994.
- [8] "AIM INFRAROT-MODULE GmbH," [Online]. Available: <http://www.aim-ir.com/en/main/products/modules.html>. [Accessed 27 August 2012].
- [9] C. Peter and G. James, *Mercury Cadmium Telluride Growth, Properties and Applications*, West Sussex: John Wiley & Sons Ltd, 2011.
- [10] A. Rogalski, *Infrared Detectors*, Boca Raton, FL: CRC Press, Taylor & Francis Group, 2011.
- [11] R. Triboulet and P. Siffert, *CdTe and Related Compunds; Physics, Defects, Hetero- and Nano-structures, Crystal Growth, Surfaces and Applications*, Oxford: Elsevier Ltd., 2010.
- [12] S. Kasap and P. Capper, *Springer Handbook of Electronic and Photonic Materials*, Würzburg: Springer Science+Business Media, Inc, 2006.

- [13] A. Datta, K. A. Jones, S. Swain and K. G. Lynn, "Modified Vertical Bridgman Growth of Cd<sub>1-x</sub>Zn<sub>x</sub>Te Detector Grade Crystal in a 4 inch EDG Furnace," in *IEEE Nuclear Science Symposium Conference*, Pullman, 2009.
- [14] C.-H. Su and S. L. Lehoczky, "Growth of CdZnTe Crystals by Bridgman Technique with Controlled Overpressures of Cd," NASA/Marshall Space Flight Center, Huntsville.
- [15] P. Capper and J. J. Gosney, "Method of Growing Crystalline Cadmium Mercury Telluride and Crystalline Cadmium Mercury Telluride Grown by the Method". Southampton, England Patent 4551196, 5 November 1985.
- [16] "University of Victoria," 2008. [Online]. Available: <http://www.cgl.uvic.ca/techniques.html>. [Accessed 27 July 2012].
- [17] G. Li, W. Jie, T. Wang and G. Yang, "Impurities in CdZnTe Crystal Grown by Vertical Bridgman Method," *Nuclear Instruments and Methods in Physics Research A*, vol. 534, no. 3, pp. 511-517, 2004.
- [18] R. Triboulet, "Fundamentals of the CdTe Synthesis," *Journal of Alloys and Compounds*, vol. 371, no. 1-2, pp. 67-71, 2004.
- [19] A. Zappettini, M. Zha, M. Pavesi, M. Zanichelli, F. Bissoli, L. Zanotti, N. Auricchio and E. Caroli, "Boron Oxide Encapsulated Vertical Bridgman: A Method for Preventing Crystal-Crucible Contact in the CdZnTe Growth," *IEEE Transactions on Nuclear Science*, vol. 54, no. 4, pp. 798-801, 2007.
- [20] M. Schieber, T. Schlesinger, R. James, H. Hermon, H. Yoon and M. Goorsky, "Study of Impurity Segregation, Crystallinity, and Detector Performance of Melt-Grown Cadmium Zinc Telluride Crystals," *Journal of Crystal Growth*, Vols. 237-239, pp. 2082-2090, 2002.
- [21] S. Sen, H. L. Hettich, D. R. Rhiger, S. L. Price, M. C. Currie, R. P. Ginn and E. O. McLean, "CdZnTe Substrate Producibility and Its Impact on IRFPA Yield," *Journal of Electronic Materials*, vol. 28, no. 6, pp. 718-725, 1999.
- [22] M. Fiederle, T. Duffar, J. Garandet, V. Babentsov, A. Fauler, K. Benz, P. Dusserre, V. Corregidor, E. Dieguez, P. Delaye, G. Roosen, V. Chevrier and J. Launay.
- [23] D. Gasperino, M. Bliss, K. Jones, K. Lynn and J. J. Derby, "On Crucible Effects during the Growth of Cadmium Zinc Telluride in an Electrodynamical Gradient Freeze Furnace," *Journal of Crystal Growth*, vol. 311, no. 8, pp. 2327-2335,

2009.

- [24] "Beijing Boyu PBN Products," [Online]. Available: <http://www.bypbn.com/page3.html>. [Accessed 19 December 2011].
- [25] K. Suzuki, H. Taniguchi, H. Kurita and R. Hirano, "CdTe Semiconductor Substrate for Epitaxial Growth and Substrate Container". Tokyo, Japan Patent EP2369041A1, 28 September 2011.
- [26] E. Weiss, "30 Years of HgCdTe Technology in Israel," *Proceedings of SPIE*, vol. 7298, pp. 72982W-1-72982W-15, 2009.
- [27] Y. Xu, W. Jie, T. Wang, P. Yu, Y. He, L. Fu and P. Sellin, "Morphology Evolution of Micron-Scale Secondary Phases in CdZnTe Crystals Grown by Vertical Bridgman Method," *Journal of Alloys and Compounds*, vol. 509, no. 5, pp. 2338-2342, 2011.
- [28] S. K. Swain, K. A. Jones, A. Datta and K. G. Lynn, "Effects of Impurities and Secondary Phases on the Performance of CdZnTe Radiation Detectors".
- [29] J. Radhakrishnan, B. Sunderseshu, M. Srivastava, G. Seth, R. Raman, R. Narula and R. Bagai, "Homogenization of Zinc Distribution in Vertical Bridgman Grown Cd<sub>0.96</sub>Zn<sub>0.04</sub>Te Crystals," *Bull. Mater. Sci.*, vol. 24, no. 6, pp. 659-663, 2001.
- [30] M. C. Duff, "Characterization of Secondary Phases in Modified Vertical Bridgman Growth CZT," *Proceedings of SPIE*, vol. 7449, pp. 74490N-1-74490N-14, 2009.
- [31] J. Zhu, J. Chu, X. Zhang and J. Cheng, "Study of Zinc Inclusions/Precipitates in CdZnTe Crystals," *Journal of Crystal Growth*, vol. 171, no. 3-4, pp. 357-360, 1997.
- [32] "National Optical Astronomy Observatory," [Online]. Available: <http://www.noao.edu/wiyn/images/fwhm.html>. [Accessed 24 August 2012].
- [33] P. Fewster and P. Whiffin, "Crystallographic Polarity and Etching of Cadmium Telluride," *Journal of Applied Physics*, vol. 54, no. 8, 1983.
- [34] K. Nakagawa, K. Maeda and S. Takeuchi, "Observation of dislocations in cadmium telluride by cathodoluminescence," *Applied Physics Letters*, vol. 34, no. 9, p. 574, 1979.

- [35] P. Brown, K. Durose, G. Russell and J. Woods, "The Absolute Determination of CdTe Crystal Polarity," *Journal of Crystal Growth*, vol. 101, no. 1-4, pp. 211-215, 1990.
- [36] F. Semendy, N. Bambha, M. C. Tamargo, A. Cavus, L. Zeng and N. Dai, "Etch Pit Studies of II-VI-Wide Bandgap Semiconductor Materials ZnSe, ZnCdSe, and ZnCdMgSe Grown on InP," Army Research Laboratory, Adelphi, 1999.
- [37] W. Everson, C. Ard, J. Sepich, B. Dean, G. Neuegebauer and H. Schaaake, "Etch Pit Characterization of CdTe and CdZnTe Substrates for Use in Mercury Cadmium Telluride Epitaxy," *Journal of Electronic Materials*, vol. 24, no. 5, pp. 505-510, 1995.
- [38] V. Dhar, A. K. Garg and R. Bhan, "Impact of CdTe/CdZnTe Substrate Resistivity on Performance Degradation of Long-Wavelength n+-on-p HgCdTe Infrared Photodiodes," *IEEE Transactions on Electron Devices*, vol. 47, no. 5, pp. 978-986, 2000.
- [39] A. Koyama, A. Hichiva and R. Hirano, "Recent Progress in CdZnTe Crystals," *Journal of Electronic Materials*, vol. 28, no. 6, pp. 683-687, 1999.
- [40] F. Bissoli, J. Weyher, A. Zappettini, M. Zha and L. Zanotti, "Revealing of Defects in CdTe Crystals by DSL Etching," *Cryst. Res. Technol.*, vol. 40, no. 10-11, pp. 1060-1063, 2005.
- [41] "Freiburg University," [Online]. Available: <http://aam.mathematik.uni-freiburg.de/IAM/homepages/alfred/BSSBBDK-schema.gif>. [Accessed 22 July 2012].
- [42] S.-f. Zhu, B.-j. Zhao, Q.-f. Li, F.-l. Yu, S.-y. Shao and X.-h. Zhu, "Modified Growth of Cd<sub>1-x</sub>Zn<sub>x</sub>Te Single Crystals," *Journal of Crystal Growth*, vol. 208, pp. 264-268, 2000.
- [43] G. Li, S.-J. Shih, S. Mu, Y. Xu and W. Jie, "Study of Te Nanoprecipitates in CdZnTe Crystals," *Journal of Materials Research*, vol. 25, no. 7, pp. 1298-1303, 2011.
- [44] J. J. Derby, D. Gasperino, N. Zhang and A. Yeckel, "Modeling the Crystal Growth of Cadmium Zinc Telluride: Accomplishments and Future Challenges," Department of Chemical Engineering and Material Science, University of Minnesota, Minneapolis.
- [45] L. P. Shcherbak, O. V. Kopach, P. M. Fochuk, A. E. Bolotnikov and R. B. James, "Thermographic Analyses of the Growth of Cd<sub>1-x</sub>Zn<sub>x</sub>Te Single

Crystals," *Proceedings of SPIE*, vol. 7805, pp. 78051B-78051B-7, 2010.

[46] "Wikipedia," [Online]. Available: <http://en.wikipedia.org/wiki/File:FWHM.svg>. [Accessed 18 August 2012].